2021-06

COMPUTATIONAL ANALYSIS OF TWIN-SKIN CLOTH SAILS FOR HIGH-PERFORMANCE SAILING VESSELS

Caraher, Sean P.

Monterey, CA; Naval Postgraduate School

NAVAL POSTGRADUATE SCHOOL

MONTEREY, CALIFORNIA

THESIS

COMPUTATIONAL ANALYSIS OF TWIN-SKIN CLOTH SAILS FOR HIGH-PERFORMANCE SAILING VESSELS

by

Sean P. Caraher

June 2021

Thesis Advisor:	Garth V. Hobson
Co-Advisor:	Maximilian Platzer
Second Reader:	Anthony J. Gannon

THIS PAGE INTENTIONALLY LEFT BLANK

REPORT DOCUMENTATION PAGE			Form Approved OMB No. 0704-0188

1. AGENCY USE ONLY *(Leave blank)*	2. REPORT DATE June 2021	3. REPORT TYPE AND DATES COVERED Master's thesis

4. TITLE AND SUBTITLE
COMPUTATIONAL ANALYSIS OF TWIN-SKIN CLOTH SAILS FOR HIGH-PERFORMANCE SAILING VESSELS

5. FUNDING NUMBERS

6. AUTHOR(S) Sean P. Caraher

7. PERFORMING ORGANIZATION NAME(S) AND ADDRESS(ES)
Naval Postgraduate School
Monterey, CA 93943-5000

8. PERFORMING ORGANIZATION REPORT NUMBER

9. SPONSORING / MONITORING AGENCY NAME(S) AND ADDRESS(ES)
N/A

10. SPONSORING / MONITORING AGENCY REPORT NUMBER

11. SUPPLEMENTARY NOTES The views expressed in this thesis are those of the author and do not reflect the official policy or position of the Department of Defense or the U.S. Government.

12a. DISTRIBUTION / AVAILABILITY STATEMENT
Approved for public release. Distribution is unlimited.

12b. DISTRIBUTION CODE
A

13. ABSTRACT (maximum 200 words)

Current efforts to reduce carbon emissions have brought a resurgence of interest in sail design. Sails could be used to supplement conventional propulsion on cargo vessels or even be used on future energy ships. Energy ships are conceptual vessels that would roam the oceans harvesting energy using hydroelectric turbines and the power developed by sails. To further the estimates of energy ship power production, a towable drag device was designed and built to provide data about the effect of a hydro-electric turbine's drag on a vessel's speed. In addition, computational fluid dynamics studies were conducted on a new twin-skin sail design to determine its potential for use on energy-ships. This twin skin sail differs from traditional sails by using two cloth elements to create an airfoil-like section with finite thickness. Both fluid-structure interaction and typical static simulations were performed. Findings show that the twin-skin mainsail aerodynamically outperforms all but two-element rigid sails. In addition, twin-skin mainsails have the ability to be reefed or completely taken down, making them more manageable in extreme weather. This performance in addition to its ease of handling makes it a good fit for use on an energy-ship. Future work should be done to analyze this design in three-dimensional flows as well as the effects of mounting multiple sails on a single vessel.

14. SUBJECT TERMS computation fluid dynamics, sails, energy ship	15. NUMBER OF PAGES 73
	16. PRICE CODE

17. SECURITY CLASSIFICATION OF REPORT	18. SECURITY CLASSIFICATION OF THIS PAGE	19. SECURITY CLASSIFICATION OF ABSTRACT	20. LIMITATION OF ABSTRACT
Unclassified	Unclassified	Unclassified	UU

NSN 7540-01-280-5500

Standard Form 298 (Rev. 2-89)
Prescribed by ANSI Std. 239-18

THIS PAGE INTENTIONALLY LEFT BLANK

Approved for public release. Distribution is unlimited.

COMPUTATIONAL ANALYSIS OF TWIN-SKIN CLOTH SAILS FOR HIGH-PERFORMANCE SAILING VESSELS

Sean P. Caraher
Ensign, United States Navy
BS, United States Naval Academy, 2020

Submitted in partial fulfillment of the
requirements for the degree of

**MASTER OF SCIENCE IN ENGINEERING SCIENCE
(AEROSPACE ENGINEERING)**

from the

**NAVAL POSTGRADUATE SCHOOL
June 2021**

Approved by: Garth V. Hobson
Advisor

Maximilian Platzer
Co-Advisor

Anthony J. Gannon
Second Reader

Garth V. Hobson
Chair, Department of Mechanical and Aerospace Engineering

THIS PAGE INTENTIONALLY LEFT BLANK

ABSTRACT

Current efforts to reduce carbon emissions have brought a resurgence of interest in sail design. Sails could be used to supplement conventional propulsion on cargo vessels or even be used on future energy ships. Energy ships are conceptual vessels that would roam the oceans harvesting energy using hydroelectric turbines and the power developed by sails. To further the estimates of energy ship power production, a towable drag device was designed and built to provide data about the effect of a hydro-electric turbine's drag on a vessel's speed. In addition, computational fluid dynamics studies were conducted on a new twin-skin sail design to determine its potential for use on energy-ships. This twin skin sail differs from traditional sails by using two cloth elements to create an airfoil-like section with finite thickness. Both fluid-structure interaction and typical static simulations were performed. Findings show that the twin-skin mainsail aerodynamically outperforms all but two-element rigid sails. In addition, twin-skin mainsails have the ability to be reefed or completely taken down, making them more manageable in extreme weather. This performance in addition to its ease of handling makes it a good fit for use on an energy-ship. Future work should be done to analyze this design in three-dimensional flows as well as the effects of mounting multiple sails on a single vessel.

THIS PAGE INTENTIONALLY LEFT BLANK

TABLE OF CONTENTS

LIST OF FIGURES

THIS PAGE INTENTIONALLY LEFT BLANK

LIST OF TABLES

THIS PAGE INTENTIONALLY LEFT BLANK

LIST OF ACRONYMS AND ABBREVIATIONS

2D	two-dimensional
3D	three-dimensional
C_l	two-dimensional lift coefficient
C_d	two-dimensional drag coefficient
FEA	finite element analysis
FSI	fluid structure interaction
GPS	global positioning system
psig	pounds per square inch gauge
NPS	Naval Postgraduate School

THIS PAGE INTENTIONALLY LEFT BLANK

ACKNOWLEDGMENTS

I would like to thank all of my advisors over the course of my research. Professor Hobson contributed heavily to ensuring the accuracy of my CFD simulations. I would also like to thank Professor Platzer for helping analyze the CFD simulations and providing insight into the aerodynamics observed.

THIS PAGE INTENTIONALLY LEFT BLANK

I. INTRODUCTION

A. PROJECT BACKGROUND

The use of sails on large vessels, including cargo ships and tankers, is not a new idea. It has been proposed countless times and many concepts for sail-assisted vessels have been proposed [1]. The use of sails may serve as a way to lower carbon emissions from large-scale shipping or even be used to harvest energy using hydrokinetic turbines [2]. Generally, the proposed concepts make use of either traditional cloth sails or articulating wing sails. However, the latest edition of the America's Cup, the most technologically advanced sailing competition, may have pioneered another sail configuration that could provide the usability advantages of cloth sails and the performance gains of a rigid wing sail [3].

B. AREAS OF RESEARCH

Two areas were seen to further this project. The first was to provide data that characterized a hydroelectric turbine's impact on a sailing ship's speed. This data is important to be able to calculate the estimated amount of power an energy ship could produce. The second area of research was to further work on multi-element sails, that sought to maximize the performance of possible sail configurations for the energy ship.

1. Energy-Ship Concept

Energy ships are designed to capture energy from sails using hydro-electric turbines. Such a ship may carry many individual sails along its length. These sails provide propulsion for the vessel. The forward motion the vessel is converted into energy by using it to drive one or more hydro-electric turbines suspended beneath the vessel. This concept allows for the generation of energy without emissions. One of the benefits of an energy ship over traditional offshore wind farms is mobility. Energy ships can travel to the areas of greatest wind speed and therefore can optimize their energy output.

There are two proposed methods of operation for an energy ship. The first is energy capture at sea that is stored in onboard batteries. This energy will be offloaded at a pier to

on-land batteries or the power grid. Another method of operation is the use of the energy to produce hydrogen onboard the energy ship. The ship would compress and store the hydrogen. When full, the energy ship would return to shore and offload its tanks of hydrogen. These two methods of operation are detailed in Figure 1.

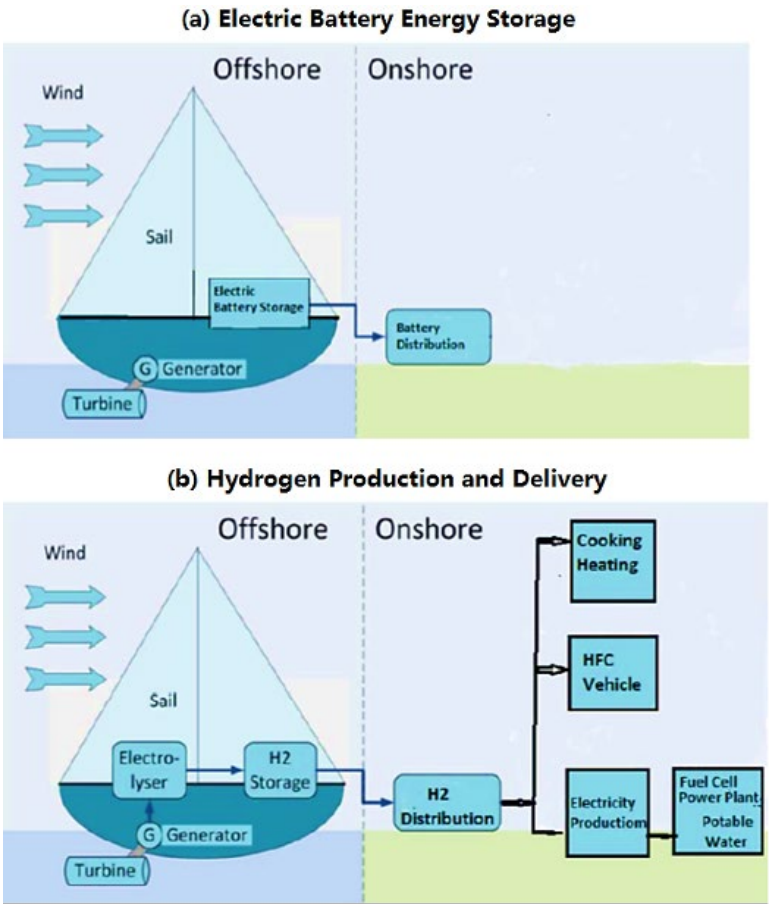

Figure 1 Two methods of energy ship operation. Source: [2].

2. Previous Sail Computational Fluid Dynamics

This thesis builds upon a previous NPS thesis written by Johnson [4]. In her work, Johnson used ANSYS CFX to produce performance estimates of two-dimensional (2D) single sail sections and 2D multi-element rigid wing, "B" and "F" in Figure 2, respectively.

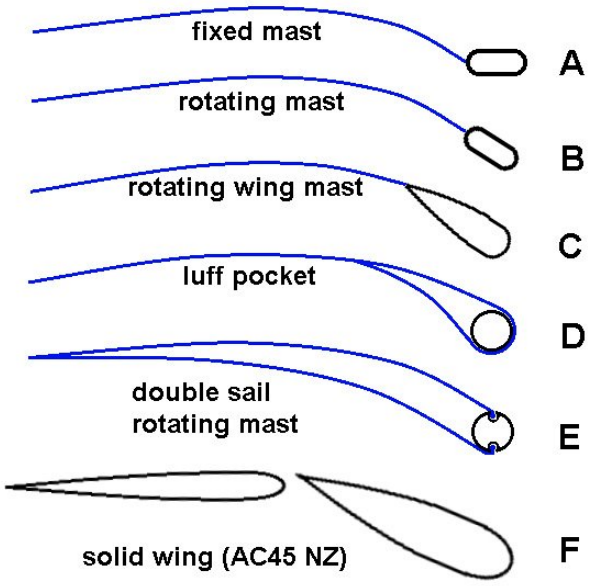

Figure 2 Different mainsail configurations. Source: [5]

C. OBJECTIVES

Overall, there are two main goals to be achieved by this research. The first is to investigate the effect of turbine drag on a sailboat. This understanding will be useful in estimating the amount of power that could be generated by a theoretical energy ship. The second goal was to explore the twin-skin mainsail concept and understand its performance. This data will provide additional data to use when deciding on a sail design for the energy ship.

THIS PAGE INTENTIONALLY LEFT BLANK

II. DRAG DEVICE

A. CONCEPTUAL DESIGN

In order to more accurately make estimations as the performance degradation of sailing ships with immersed hydro-electric turbines, the creation of a device to obtain experimental data to characterize how such a device a would affect a sailboat's speed was necessary. To provide this dataset it was determined that a tow rig would have to be built to simulate the drag of an operational hydro-electric turbine. The general plan was to retrofit a previous Naval Postgraduate School (NPS) project's catamaran with a device to simulate the drag produced by a hydro-electric turbine [6]. The rig would be anchored to the test sailboat with a load cell so that the drag it produced could be measured. To produce drag the test rig would have interchangeable flat plates so that different sizes of turbines could be simulated. The plate was to be capable of being extended and retracted into the water remotely to allow quick acquisition data. A conceptual diagram of this setup is shown in Figure 3.

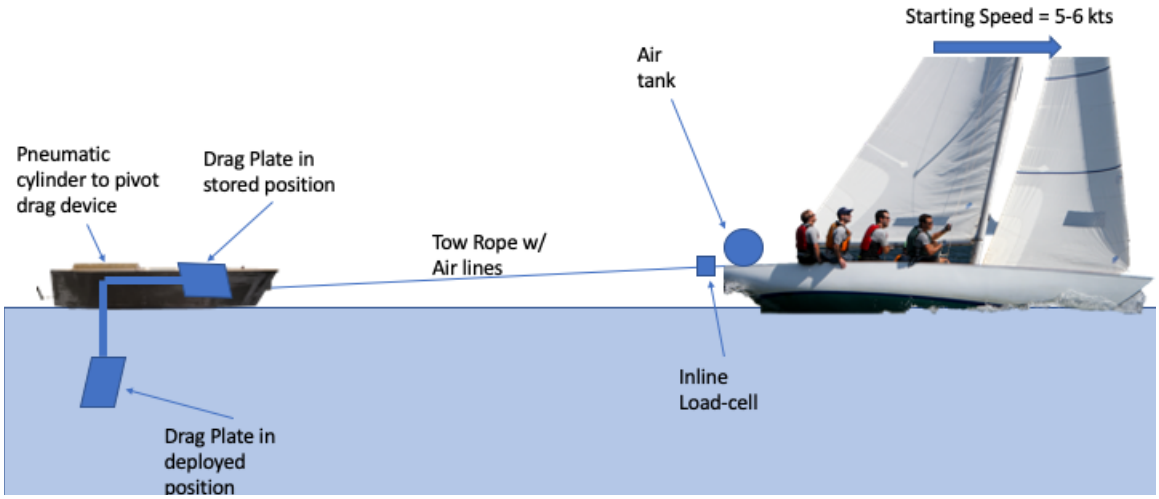

Figure 3 Experimental setup of drag device

B. DETAIL DESIGN

The design for the device was modeled in Solidworks 2019 and makes use of 2.54 cm (1 inch) x 5.08 cm (2 inch) angle aluminum that was already available at the Turbo-propulsion laboratory. The three-dimensional (3D) model of the design of the tow rig is shown in Figure 4. It reuses the hulls from the catamaran, but all the structure is to be constructed new. Detailed drawings of the design of the test apparatus are shown in Appendix A.

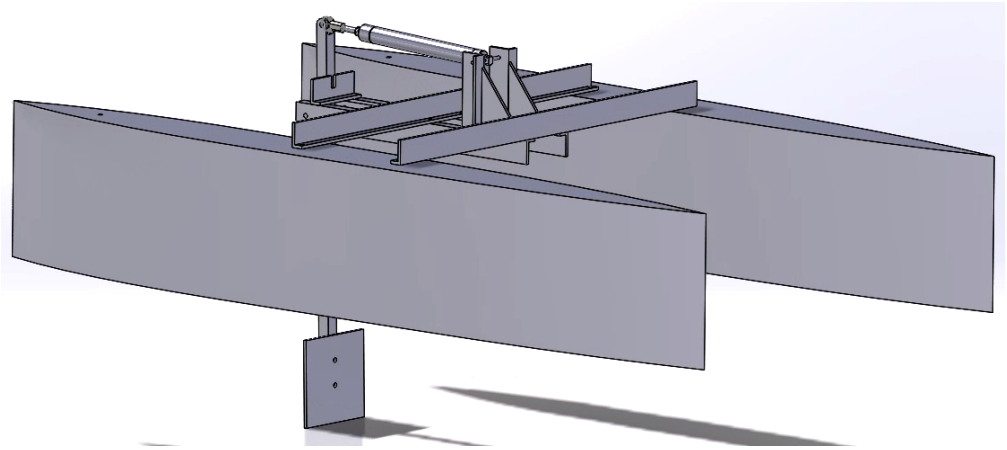

Figure 4 Solid model of drag device with drag plate extended

The drag plate was sized to provide approximately 88.96 Newtons (20 pounds) of drag at 6 knots of speed through the water, calculations are shown in Appendix B. The drag plate will be extended and retracted by means of a double-action pneumatic cylinder. The cylinder is fed from an air tank that will be mounted onboard the test sailboat. The hoses will run along the tow rope from the sailboat to the drag device as a sort of umbilical. Using a 37.85 liter (10-gallon) air tank charged initially to 10.34 bar (150 psig), the system should be capable of raising and lowering the drag plate 40 times before having to be charged, according to MATLAB simulations shown in Appendix C. Figure 5 shows the estimated drop in system pressure as the cylinder is extended and retracted, until it reaches the limit pressure at which the cylinder will no longer be able to raise the drag plate due to forces on the plate.

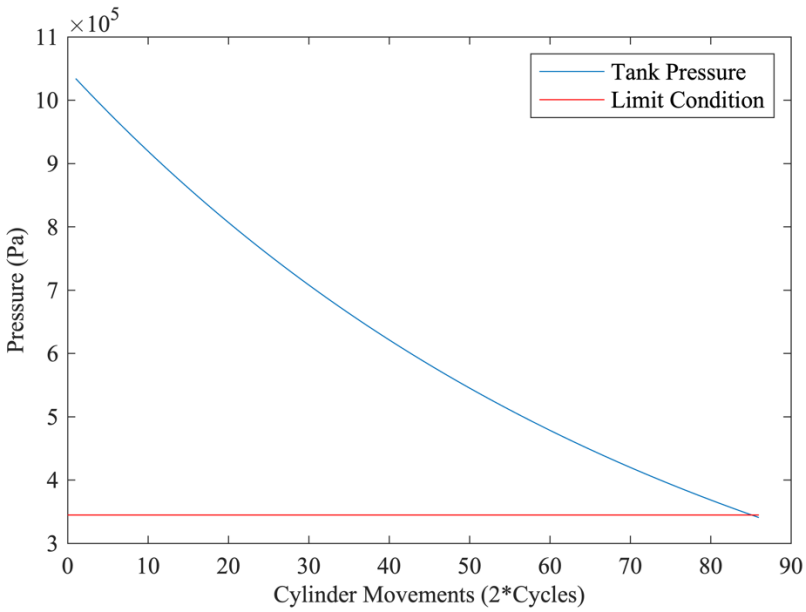

Figure 5 System pressure as a function of pneumatic cylinder movements

C. DATA ACQUISITION

Drag force will be measured by means of a 222.4 Newton (50 lbf) Honeywell load cell mounted on the tow vessel and powered by a 12-volt motorcycle battery. A National Instruments data acquisition model will be used to read the load cell voltage and transfer the data to a laptop running MATLAB [7]. Both pieces of hardware are shown in Figure 6.

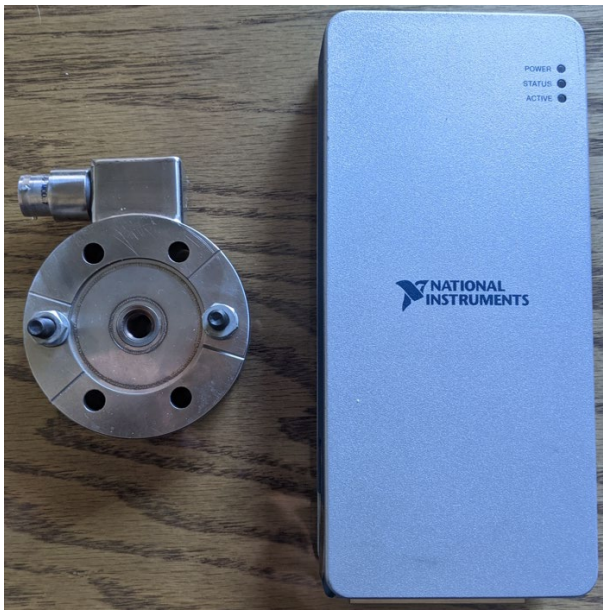

Figure 6 Honeywell loadcell (left) and National Instruments data acquisition module (right)

To collect wind speed and wind angle data, the tow sailboat's onboard instrumentation will be used. Speed data will be collected in two forms: speed through the water and speed over ground. Speed through the water will be measured by the tow sailboats onboard instrumentation and speed over ground will be measured by handheld GPS.

D. TEST PLANS

When completed the drag device will be towed behind two different sailboats, a Shields class sloop and a J/80 keelboat. These boats are shown in Figure 7 and Figure 8, respectively. This should provide data that spans multiple hull designs and be more useful to predicting energy-ship performance. The ability for the drag plate to be cycled through is up and down position approximately 40 times will allow multiple data points to be collected before the tow vessel will have to return to the pier. These data points will be of varying true wind angle and sail configuration to see how these factors influence the vessel's ability to maintain speed through the water with increased drag. The apparatus, Figure 9, currently under construction and has been delayed due to parts acquisition.

Figure 7 Shields class sailboat. Source: [8].

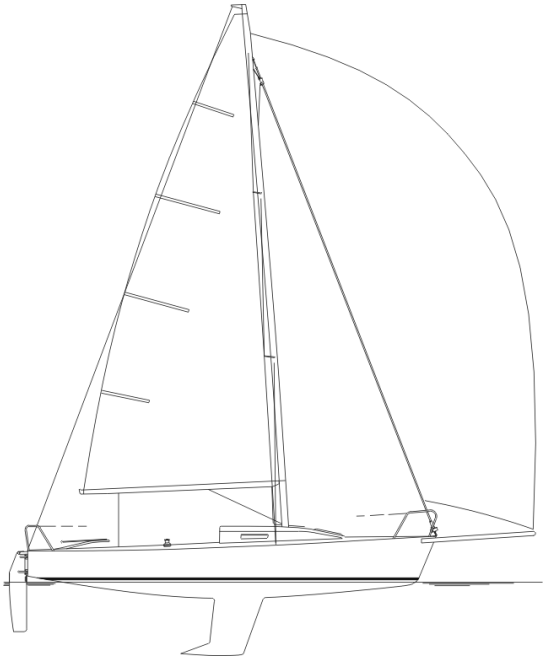

Figure 8 J/80 sailboat. Source: [9].

Figure 9 Current status of the construction of the drag device

III. FLUID STRUCTURE INTERACTION

The objective of CFD investigation was to demonstrate ANSYS workbench's two-way fluid-structure interaction capabilities. The main objective of these test cases was to test and master fluid structure interaction (FSI). This investigation is limited to two-dimensional (2D) to simplify setup and to allow faster simulations. However, the knowledge from this case will be used in future thesis work to analyze more complex FSI cases.

A. TWO-WAY FSI

Two-way FSI is a subset of typical FSI. FSI models the effect of aerodynamic loads on an object and the deformations that these loads create. Two-way FSI takes this process further passing information back and forth between fluid and structural models until surface pressures and deformations reach convergence. This requires the solution to undergo many iterations until the data transfers between the structural and fluid solvers converge. Two-way FSI has previously been completed on sails. However, the only previous attempts using ANSYS CFX used specialty wrapper codes to pass pressure and deformation data back and forth [10]. FSI is generally only used to characterize downwind sails because their flying shape is much different from their design shape due to their unsupported nature [11].

1. Setup in ANSYS Workbench

To conduct two-way FSI in ANSYS workbench, CFX and static-structural were connected with the system coupling block. All cases were run with a single coupling step because this model is not transient. However multiple coupling iterations were necessary to reach convergence. Convergence was set to 0.001 for both the pressure and deformation data transfers. To increase the stability of the model, the force data transfer was ramped in over the first five coupling iterations. This discourages the structural model from failing or generating large deformations that would cause large changes to the flow. Figure 10 shows this setup. This setup shows two CFX blocks, the first is the block for the FSI and the second obtains the solution for the undeformed shape.

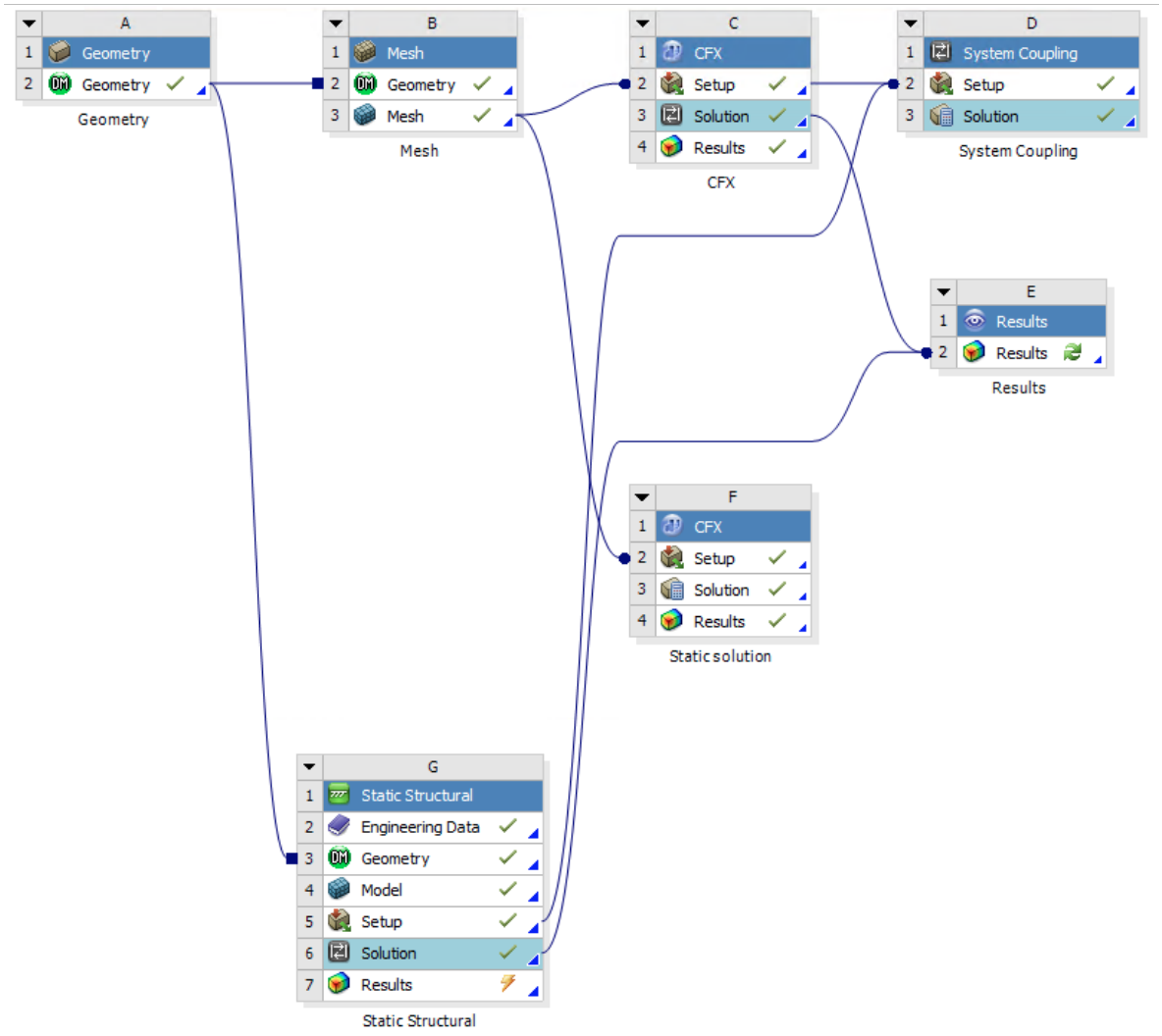

Figure 10 Workbench schematic for traditional mainsail

a. Static Structural

In ANSYS Static Structural the surface that is interacting with the fluid must be specified as a fluid solid interface. This flags this boundary to the solver as a location that should send and receive data using System Coupling as a surface that create data transfers between the connected subsystems, CFX and Static Structural. This setting is applied like any other load would be applied in Static Structural.

To constrain the sail during finite element analysis (FEA) simulation, pinned supports were integrated into the geometry, shown in Figure 11. These constraints were

implemented at both the leading and trailing edge. They carry the aerodynamic loads while allow the ends of the sail to freely rotate.

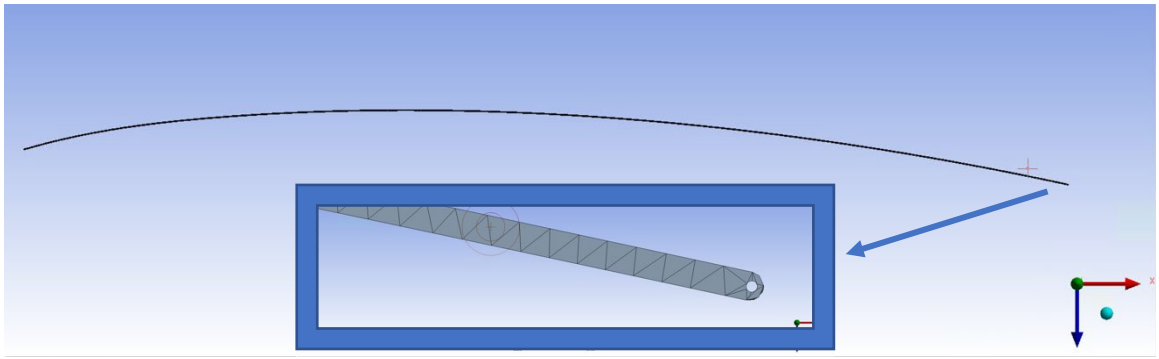

Figure 11 Pinned constraint in ANSYS static structural

b. CFX Setup

For the most part, FSI is configured in CFX-Pre identically as a typical CFX run. There is one key difference that must be enabled for the solver to be able to deal with deformations between iterations. In the basic setting for the domain, mesh deformation must be enabled with the settings shown in Figure 12. This setting creates a new parameter that must be set for each boundary condition. This new setting defines how each boundary condition will be deformed. To set these, the boundary condition that contains the fluid solid interface must be specified as "System Coupling," shown in Figure 13. Any boundary condition that intersects with the fluid structure interface must be set to "Unspecified," shown in Figure 14. In this case, the symmetry planes receive this designation so that they can conform to the deformations of the sail. All other boundary conditions should be specified as "Stationary."

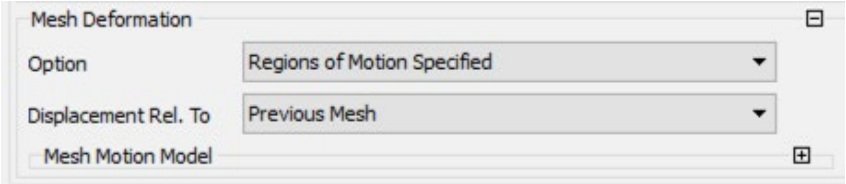

Figure 12 Mesh deformation settings in CFX-Pre

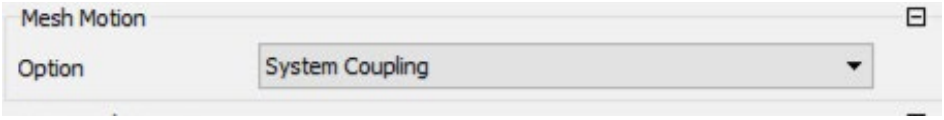

Figure 13 Mesh motion setting for the fluid structure interface

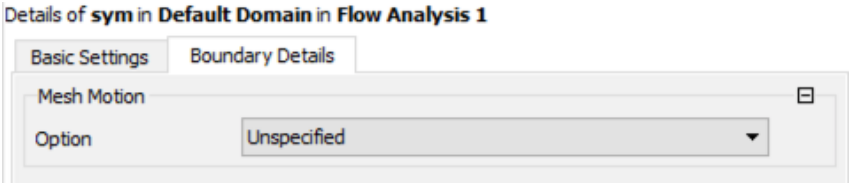

Figure 14 Mesh motion setting for the symmetry planes

c. Data Transfer Setup in System Coupling

The system coupling block shown in Figure 10 handles the setup of data transfers between ANSYS CFX and Static Structural solvers. This block contains all the settings necessary to setup an FSI run. Data transfer setup specifies what data should be passed between solvers as well as the convergence criteria for these transfers. The final important setting is the ability to ramp the data transfer. It was found that ramping the forces sent to the structural solver minimized unstable behavior and large deformations from occurring in the initial few iterations. The setting used for this study are shown in Figure 15 and Figure 16.

Property	Value
Source	
Participant	CFX
Region	sail
Variable	Force
Target	
Participant	Static Structural
Region	Fluid Solid Interface
Variable	Force
Data Transfer Control	
Transfer At	Start Of Iteration
Under Relaxation Factor	1
RMS Convergence Target	0.001
Ramping	Linear to Minimum Iteration

Figure 15 Data transfer settings from CFX to static structural

Property	Value
Source	
Participant	Static Structural
Region	Fluid Solid Interface
Variable	Incremental Displacement
Target	
Participant	CFX
Region	sail
Variable	Mesh Displacement
Data Transfer Control	
Transfer At	Start Of Iteration
Under Relaxation Factor	1
RMS Convergence Target	0.001
Ramping	None

Figure 16 Data transfer settings from static structural to CFX

2. Difficulties Meshing with Shell Elements

A sail is generally made of cloth and therefore is incapable of supporting compression loads. Therefore, for an accurate structural model of a sail to be created this property must be enforced. This can be implemented in ANSYS structural by using shell elements to mesh a surface that represents the sail. These elements are two-dimensional but can have a finite thickness assigned to them. In addition, ANSYS provides the "membrane" stress setting that enforces the rule that only tension can be supported.

Initial attempts of simulating FSI using ANSYS workbench used this method to mesh the sail for structural analysis. However, the solution was often unstable and caused the solver to crash with errors. If a solution was obtained, it resembled that shown in, Figure 17, which is not likely to be correct.

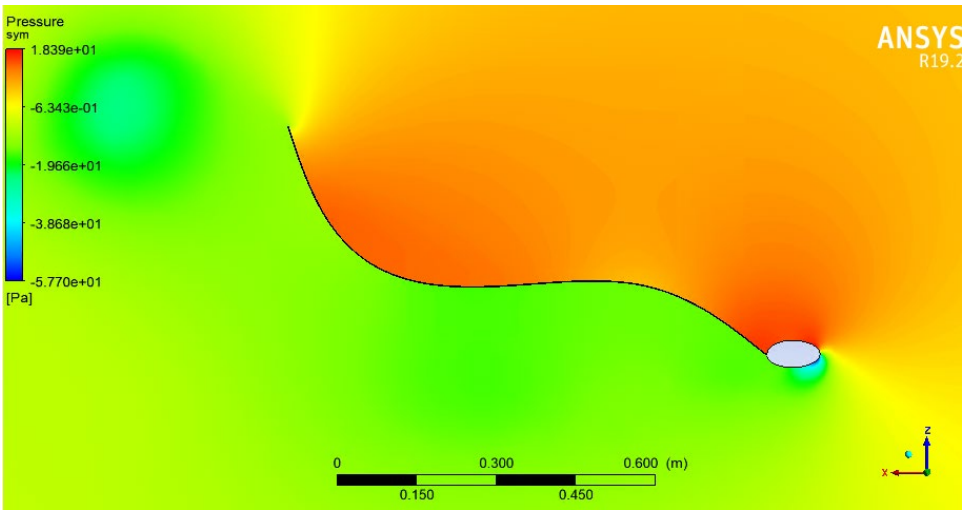

Figure 17 Result using shell elements

Many iterations of this setup with shell elements were attempted, but a stable result could not be achieved. Future attempts at FSI were all done using solid elements that can carry both tension and compression. This is not physically correct but is deemed reasonable because the thickness of the sail was only 1mm which should minimize its resistance to bending.

B. TRADITIONAL MAINSAIL

The first setup tested using this FSI structure was a traditional cloth mainsail and elliptic mast section. The geometry was designed to allow for 2D analysis in CFX. The starting sail shape is an arbitrary spline with maximum camber far forward. This is shown in Figure 18. Sail thickness was 1 millimeter, and the material was modeled as nylon with Young's modulus of 3200 MPa and a Poisson's ratio of 0.2 [10]. The sail was given a 1-meter chord and 10% camber.

Initial runs of this geometry were done without FSI to determine optimum angles for the sail and mast to reduce flow separation. Without rotating the mast, circulation around the sail caused massive flow separation on the suction side causing difficulties in resolving the solution. The FSI run took 15 iterations to reach pressure, deformation and CFX convergence as shown in Figure 19. The conditions for this test are shown in used Table 1. Turbulent kinetic energy and dissipation modeling ($\kappa-\varepsilon$) was used for these tests.

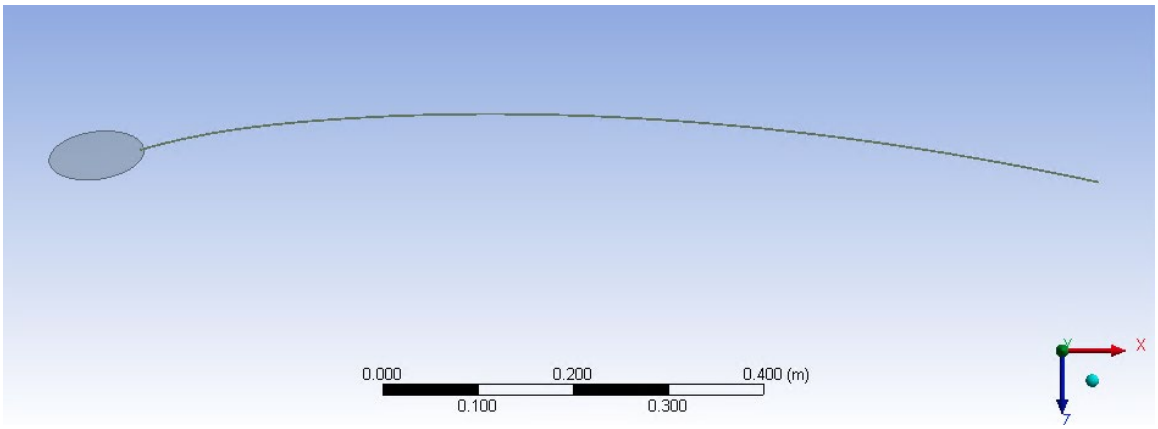

Figure 18 Initial geometry for traditional mainsail

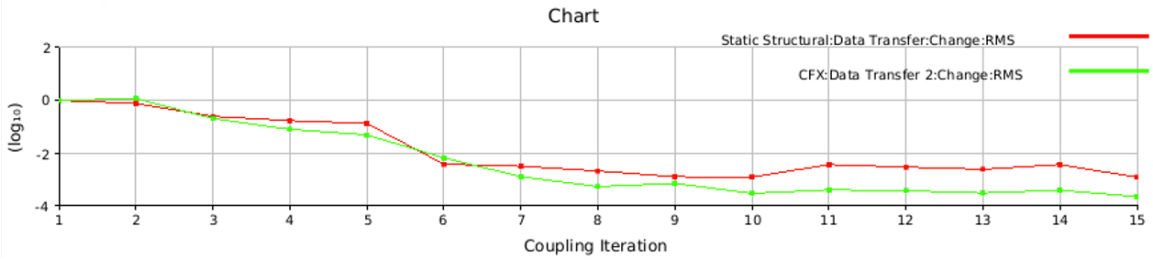

Figure 19 Convergence of surface pressures and sail deformation

Table 1. Traditional mainsail test conditions

Angle of Attack	2 degrees
Mast Rotation	8 degrees
V ∞	20 knots

This simulation showed flow attachment over most of the mainsail. Only in the wake of the mast section does the flow separate, however this simulation shows that these sections reattach quickly, shown in Figure 20. For the design of the energy-ship fairings in this area or a more streamlined mast section may be useful if a traditional sail is to be used.

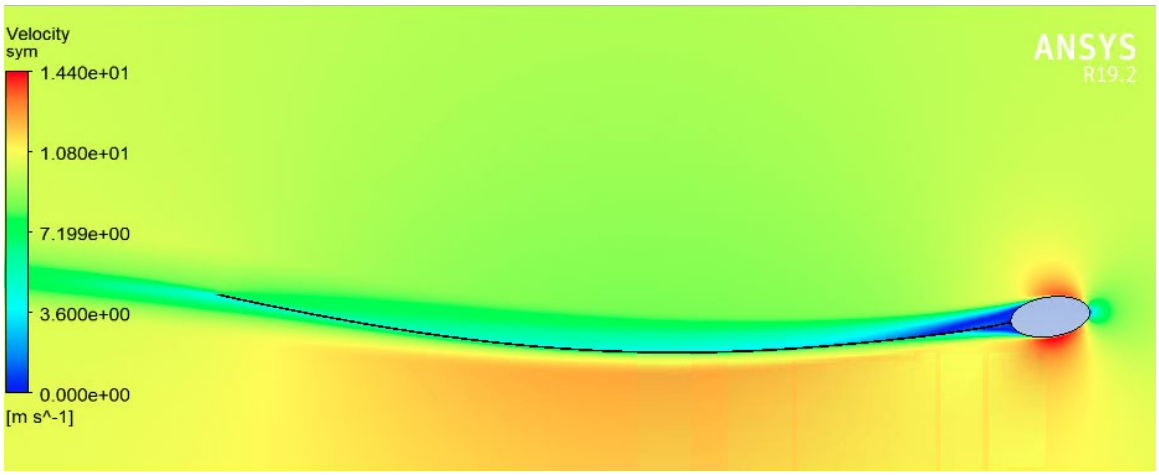

Figure 20 Velocity field around deformed single sail

Deformations were small as the sail did not stretch much, however the location of maximum draft was observed to move towards the trailing edge. The deformed shape produced more lift than the initial shape. This is shown in Figure 21.

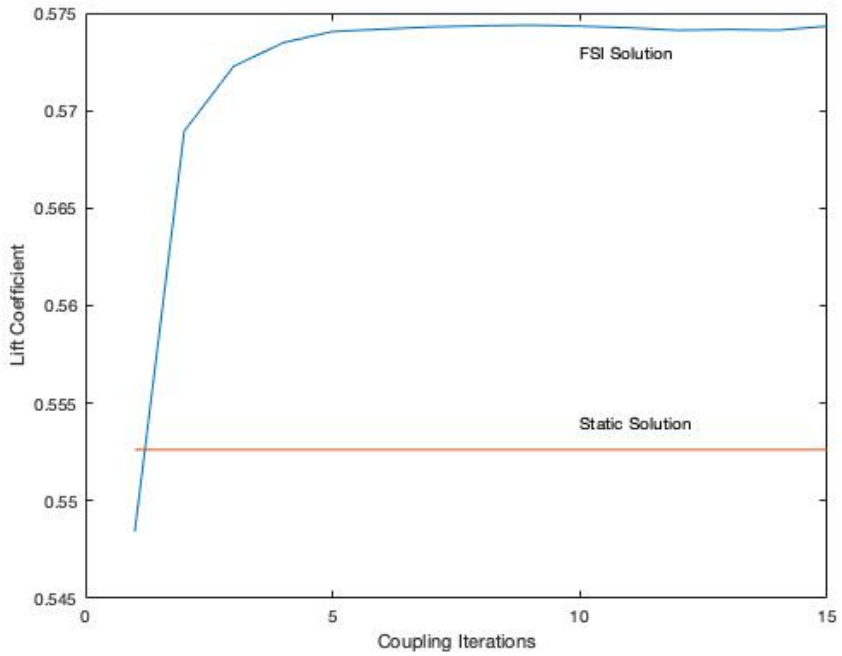

Figure 21 Change in C_l with coupling iterations for traditional mainsail

C. TWIN SKIN MAINSAIL

Once the traditional mainsail was working the next step was to attempt more complex designs. The inspiration for this sail setup is the AC75 class sailboats. They use "D" section masts with two sails to create a more airfoil like shape with finite thickness. The geometry that was used for the analysis is shown in Figure 22. Both sails have equal arc length as to be physically accurate to how this system would operate if built. The same material was used as was for the traditional mainsail. The twin skin mainsail is discussed and developed further in Chapter IV of this report.

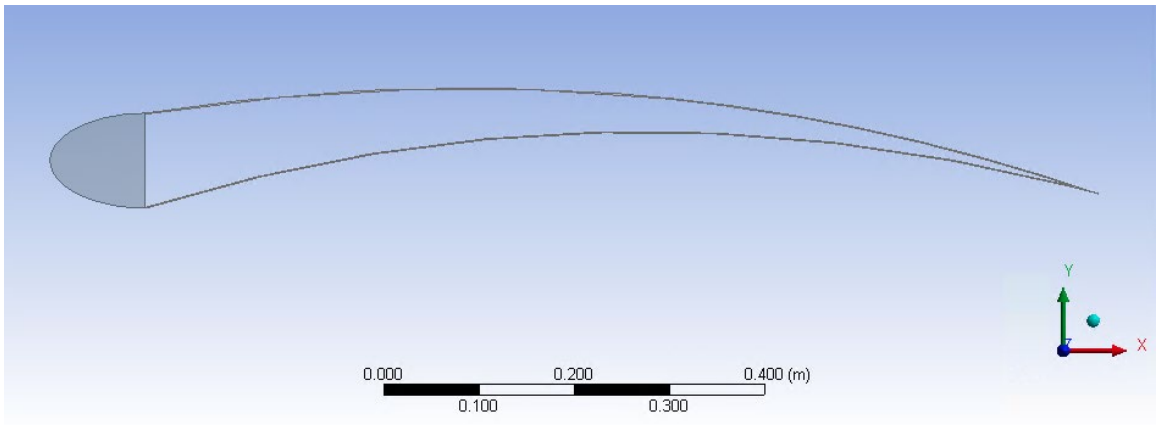

Figure 22 Twin-skin mainsail geometry with elliptic "D" section mast

This design was run at the same angle of attack and velocity as the traditional mainsail. However due to time constraints the mesh was less detailed to reduce computational expense. The mesh contained 115,026 nodes and 56,362 elements and did not include inflation layers. The mast was given a surface roughness of 0.001m to ensure the boundary layer was turbulent over the sail and to promote flow attachment. $\kappa-\varepsilon$ turbulence modeling was used for these calculations.

Figure 23 shows the resulting flow field. There is slight separation that occurs on the lower surface as the flow transitions from the mast section to the nylon sail. Future designs should look to rotate the mast section to prevent this discontinuity from being present. This model however shows the flow quickly reattaching.

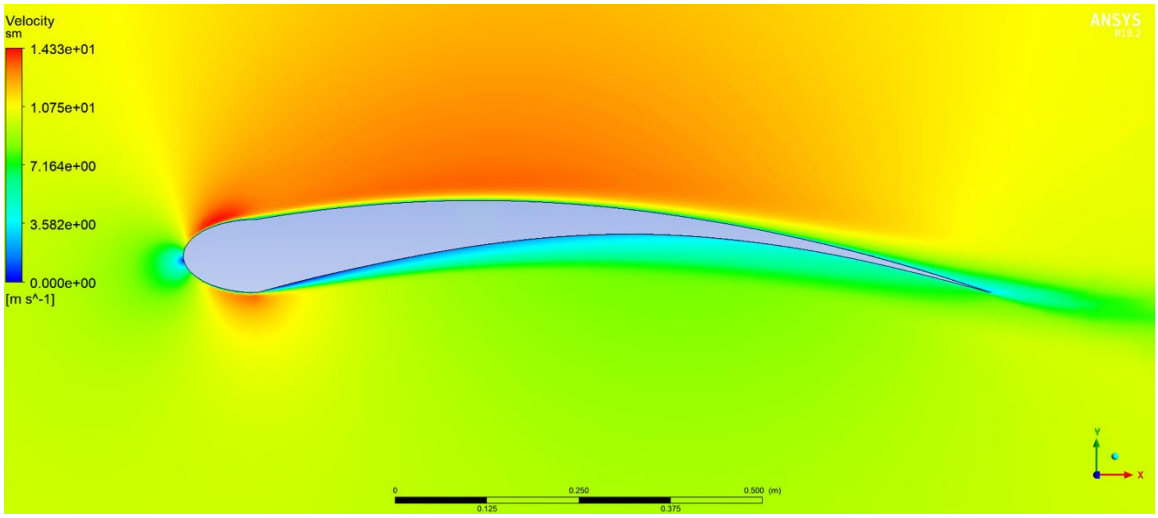

Figure 23 Velocity field around deformed twin skin mainsail

The twin skin mainsail generated a higher lift coefficient at the same angle of attack as the traditional mainsail. As for deformations, they were small but observation showed that the lower surface's draft moved towards the trailing edge and the upper surface's draft moved forward. Similar to the traditional mainsail this new shape produced more lift than the undeformed sail. This phenomenon is shown in Figure 24 the upper line shows the change in lift as coupling iterations progress, while the red line shows the lift produced by the initial shape.

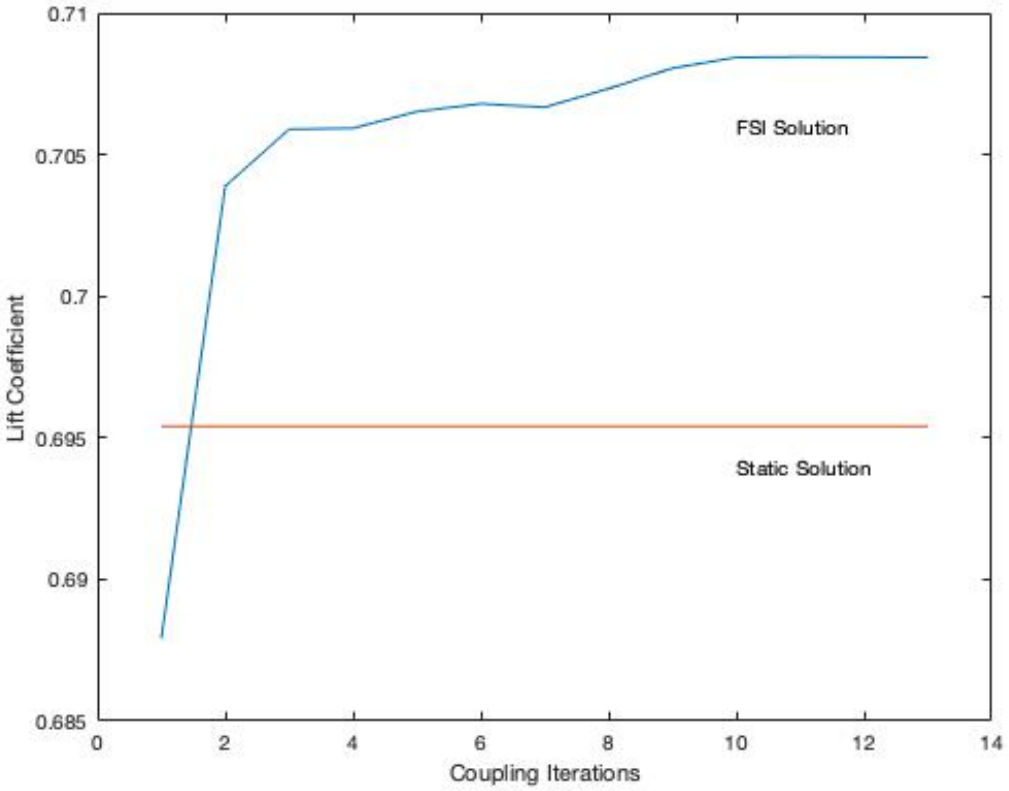

Figure 24 Change in C_l with coupling iterations for twin-skin mainsail

D. SUMMARY

FSI in ANSYS Workbench appears to be functioning correctly. The setup of this project will be useful for future more complex 2D geometries and possible 3D simulations. The deformations that were captured in these two test cases seem accurate but have not been compared to any other data or real-world tests. The modeling of the sails mechanical properties is as if the sail was a solid piece of nylon, which can provide some bending rigidity unlike cloth. Therefore, accuracy of these simulations should be questioned. Future simulations will have to be run with more detailed meshes and inflation layers in order to accurately predict the drag of these setups. Drag is important for calculating the thrust force generated by each sail configuration. Despite the limitations of this study, the lessons learned doing these simulations will serve as a stepping off point for future thesis work.

Computational expense is the main factor that limits the use of FSI in the analysis of sails. Since each simulation require at least ten iterations to reach convergence computational time is at least ten times that of a static solution. For a single case this may be acceptable. However, if angle of attack sweep needs to be conducted the computational time needed for FSI is unrealistic. For this reason, further development of the twin-skin mainsail was conducted using traditional static CFD.

IV. TWIN-SKIN MAINSAIL

A. HISTORY

The America's Cup has long been the pinnacle of high-performance sailboat design. Ever since the cup was first competed for in 1851, by the "radical" looking schooner America, the race has produced innovations in high performance sailboat design. Rigid wing sails were first introduced to the Cup in 1988 by Dennis Connor's syndicate. More recently wing sails have been used onboard the AC72 and AC50 catamarans [3]. These rigid wing sails are composed of multiple elements that can be articulated to create efficient multi-element airfoil sections. Figure 25 shows four different designs of rigid wing sails used by teams on their AC72 catamarans. These sails produce incredible performance for both the AC72 and AC50 classes; however, they are held back by the difficulty of handling a rigid wing. For safe storage these large wings must be taken down in order to prevent them from being damaged by winds while not being used. Their construction generally is very light using an inner carbon structure with a mylar covering. The process of taking one of these sails down took 30 to 40 people approximately one hour with the aid of a large crane in the case of the AC72 wing, shown in Figure 26 [12]. In addition, unlike traditional cloth sails, rigid wing sails cannot be reduced or reefed as wind speed increases, which could leave a vessel in a dangerous situation in adverse weather conditions.

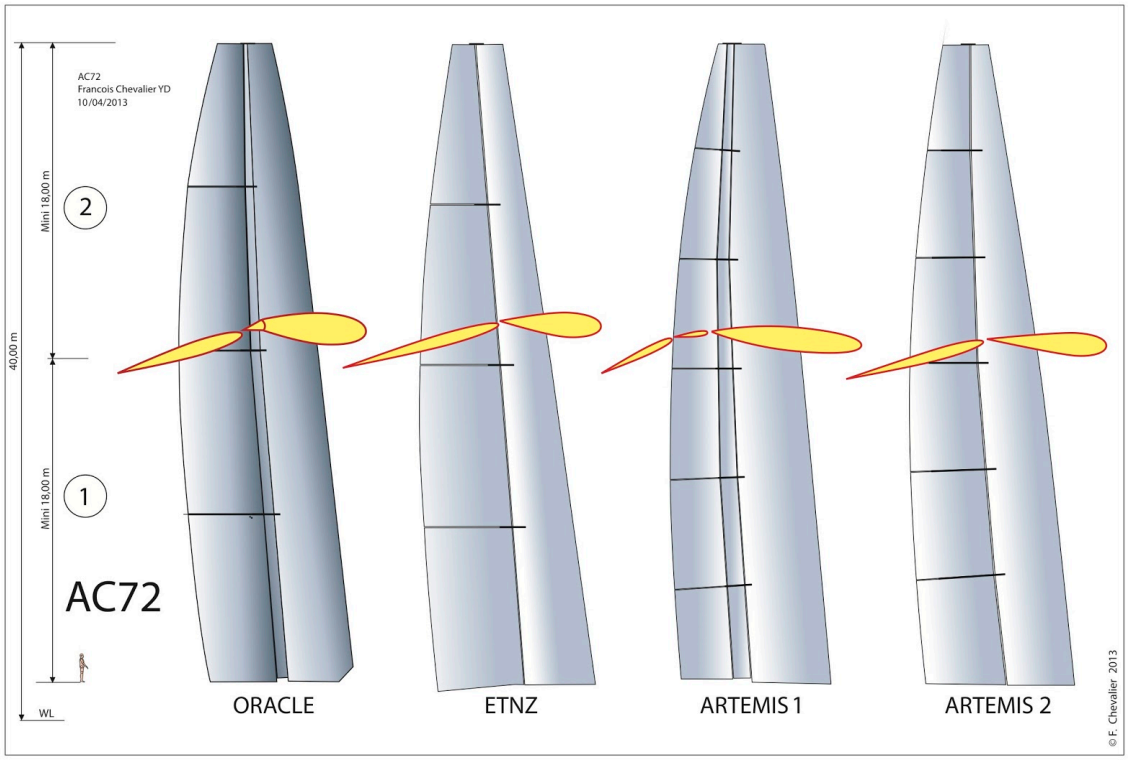

Figure 25 Configuration of AC75 rigid wing sail. Source: [13].

Figure 26 AC72 mast stepping operation. Source: [12].

These difficulties as well as the increased cost and technical complexity pushed America's Cup organizers to specify the use of a twin-skin mainsail for the 36th America's Cup. Twin-skin mainsails are not a new concept, however. The idea was first filed for patent by the famous sailboat designer Lewis Herreshoff in 1925 [14].This design uses two cloth sails that are attached to an elliptic mast section to create an airfoil like shape with finite thickness. The aerodynamic performance of this sail configuration is mostly unknown because most of the development of twin skin mainsails was done in secrecy by teams competing in the 36th America's Cup. However, these designs seem to promise greater performance than traditional cloth sails without the hassle of a fully rigid wing.

These characteristics also make a rigid wing sail undesirable on an energy ship. Though these sails provide high performance, energy ships must be resilient to operate at sea for extended periods. Any damage to these sails during an energy ships operation could reduce the power output of the vessel. In a worst-case scenario, an energy ship with a rigid wing sail that is caught in a gale may be lost.

To get estimates of the performance that can be expected from these twin-skin mainsail sections, a CFD study was conducted on a representative two-dimensional twin-skin mainsail section. Analysis was conducted two dimensionally using ANSYS CFX software. The section selected was designed to represent what a twin skin mainsail may look like when hoisted. This chapter will present the results of this modeling and the challenges experienced while attempting to accurately predict the aerodynamic characteristics of the twin-skin mainsail.

B. GEOMETRY

The section was designed around the use of an elliptic mast section that would serve as the leading edge of the section. In practice this mast section would be designed to rotate to present a smoother airfoil like section for varying angles of incidence. This technique is already used onboard high-performance sailboats and has proven its feasibility in numerous circumnavigations. The sails are the connected to the mast section on either outboard edge. Each sail is of identical chord length so that the configuration can be articulated to accommodate sailing on either tack. To induce camber in this section while imposing the

condition that each sail is of equal length, the trailing edges are designed to slide over one another. This artificially allows the leeward side of the setup to be moved towards the mast inducing camber into the suction side of the sail. This geometry is shown in Figure 27. For ease of meshing and to minimize local flow separation, an angled trailing edge treatment was used, shown in Figure 28. This close up also shows in detail how the upper sail is allowed to move forward to induce camber and account for mast rotation. This case rotates the mast section six degrees.

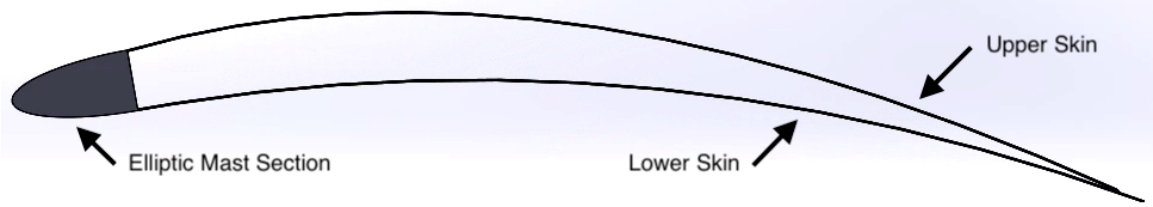

Figure 27 Twin-skin geometry using elliptic mast section

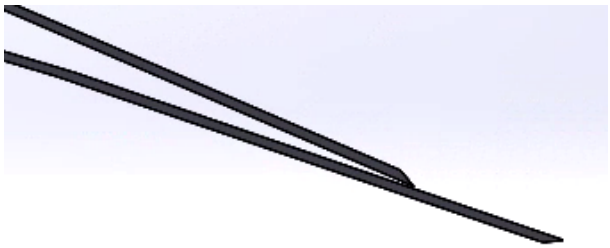

Figure 28 Trailing edge treatment on twin-skin mainsail

This geometry aims to replicate an airfoil like shape within the constraints of the twin-skin system. As shown in Figure 27, the overall shape of this twin-skin sail section resembles that of a highly cambered airfoil. There are two areas that separate it from typical airfoil sections. Due to the constraints of the twin-skin system, the interface between the upper surface and the elliptic mast section is not smooth and instead contains a slope continuity. This area is detailed in Figure 29. The second area that differs from a typical airfoil is the stepped trailing edge caused by the upper skin being allowed to slide forward along the lower, see Figure 28. The thickness of each sail is 1.5mm.

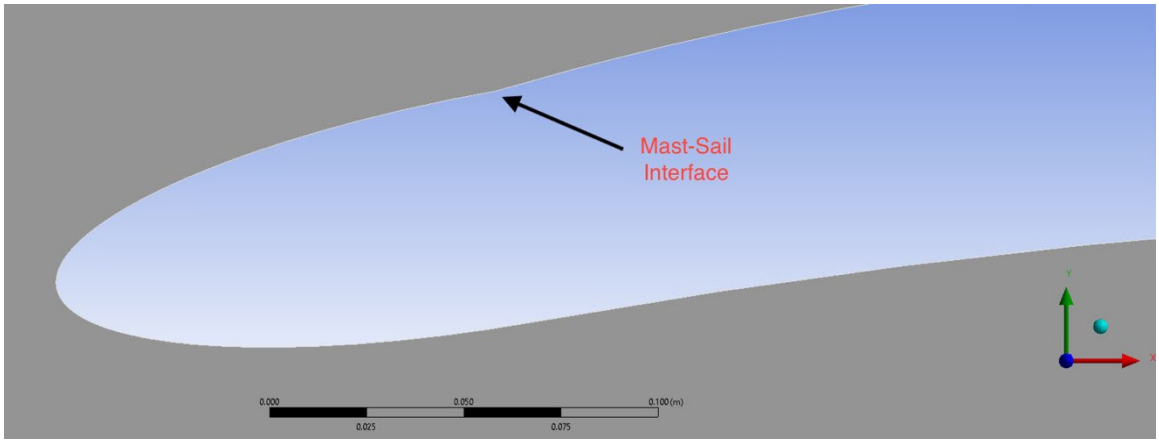

Figure 29 Detail of discontinuity at mast-sail interface

C. DOMAIN ENLARGEMENT STUDY

The nature of boundary conditions in CFD simulations requires the edges of the computational domain to be sufficiently far away from the object being tested. To find a domain size, a simple square domain was created around the proposed geometry. Domain size was slowly increased, and aerodynamic coefficients were monitored. To minimize computational time a small range of angles of attack were chosen for analysis at each domain size. The model was run with inflation layers clustered around the sail providing a Y^+ of approximately one across the entire sail. Y^+ is a non-dimensional distance from wall boundary conditions calculated based on turbulent skin-friction on the wall. Detail of the mesh surrounding the sail is shown in Figure 30. For this study, $\kappa-\varepsilon$ turbulence modeling was used to provide a fully turbulent solution.

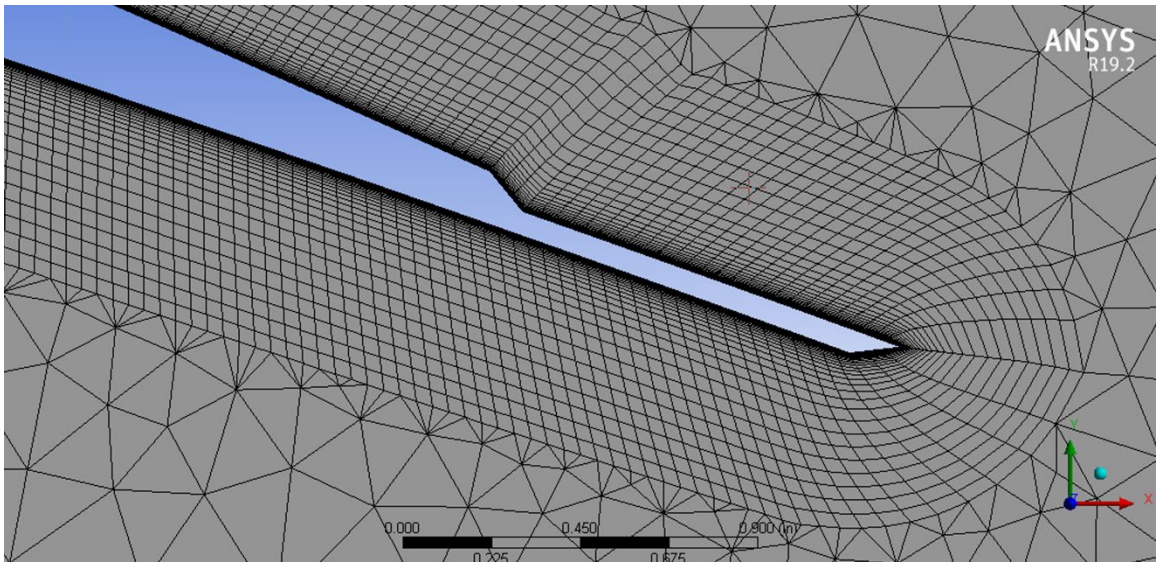

Figure 30 Detail of mesh showing inflation layers around the trailing edge

As domain size was increased, measured as the distance to the boundary from the sail, the lift coefficient begins to asymptote as the boundary distance reaches 70 meters, shown in Figure 31. In addition, the variation of velocity at the outlet of the domain was deemed to be sufficiently small and is shown in Figure 32. This leads to a 140m-by-140m domain around the twin-skin sail. When meshed, this domain contains 1,212,220 nodes and 1,127,052 elements. From this exploration, it was decided that all future simulations would be conducted with this domain size.

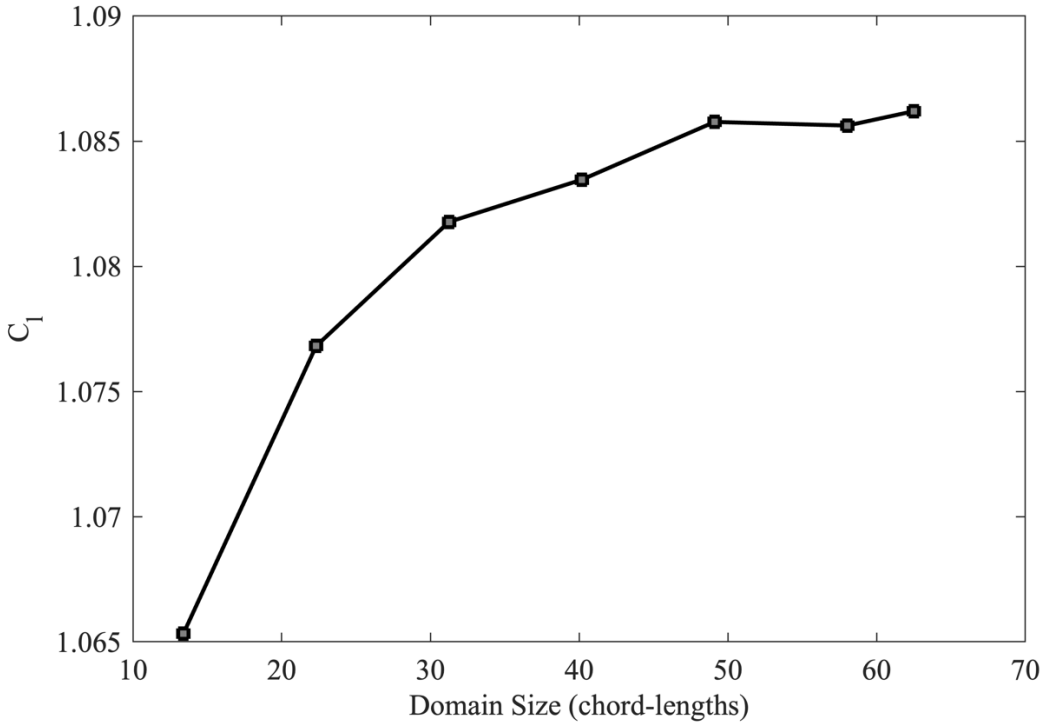

Figure 31 Lift coefficient at 2 degrees angle-of attack, Re=2,000,000

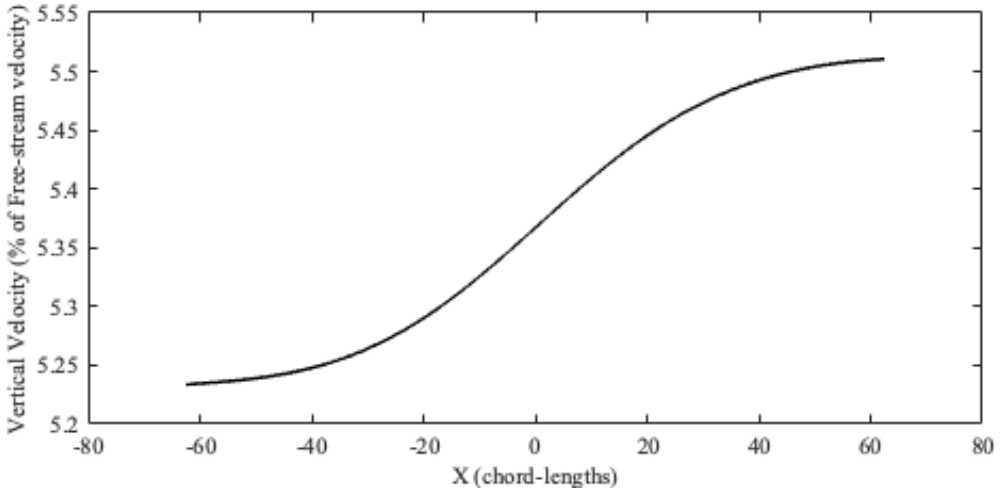

Figure 32 Vertical velocity on the entrainment boundary for 2 degrees angle-of-attack

D. CFD SETUP

From the domain size determined, two different CFX jobs were created. Both jobs used the same mesh that was used in the 140m-by-140m case from the domain study. The only difference between them was turbulence modeling. The first job used κ–ε turbulence with scalable wall functions. The second used Shear Stress Transport with Gamma Theta transition. The boundary conditions are shown in Figure 33. The angle of attack was specified by changing the u- and v-velocity at the inlet boundary condition, which was spread across two faces. An entrainment boundary condition was located at either the top or the bottom of the domain depending on the angle of attack to allow for circulation affects. These CFD runs were run at a Reynold's number of 2,000,000.

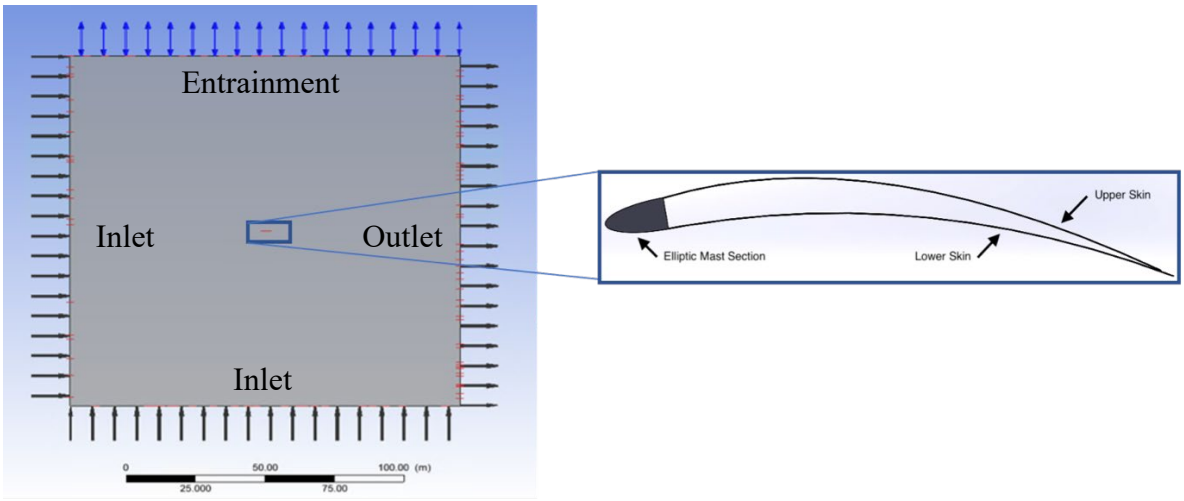

Figure 33 Configuration of boundary conditions

E. RESULTS

For each angle of attack, the force function in CFD Post was used to obtain the x and y forces on the sail. These forces were interpreted into lift and drag. Results were then non-dimensionalised and converted into aerodynamic coefficients.

1. Aerodynamic Coefficients

There are stark differences that appear when k-epsilon and SST are compared. The lift coefficients from each turbulence model are shown in Figure 34. Lift coefficients for the fully turbulent case show a smooth increase, ending in a benign stall. The transition model interestingly shows a hitch in the lift curve just before five degrees angle-of-attack. This decrease in lift coincides with a large increase in drag, shown in Figure 35.

Near stall the SST model appears to trouble resolving flow separation and this behavior is not physical, but likely just a break down in the model. It repeatably alternates between total flow separation and partial stall. This phenomenon is shown in the jagged lift curve between 12 and 15 degrees angle-of-attack and below -4 degrees angle-of-attack.

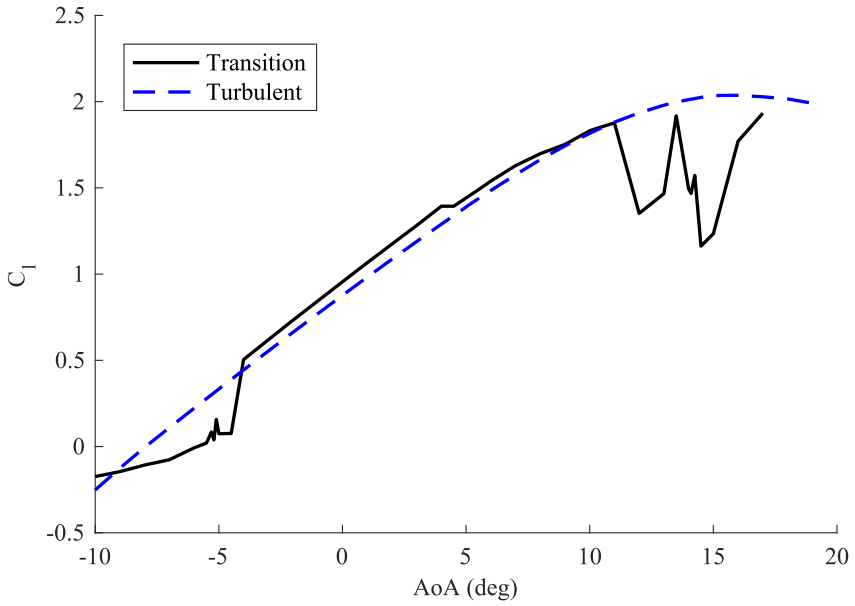

Figure 34 C_l comparison between fully turbulent and transition modeling

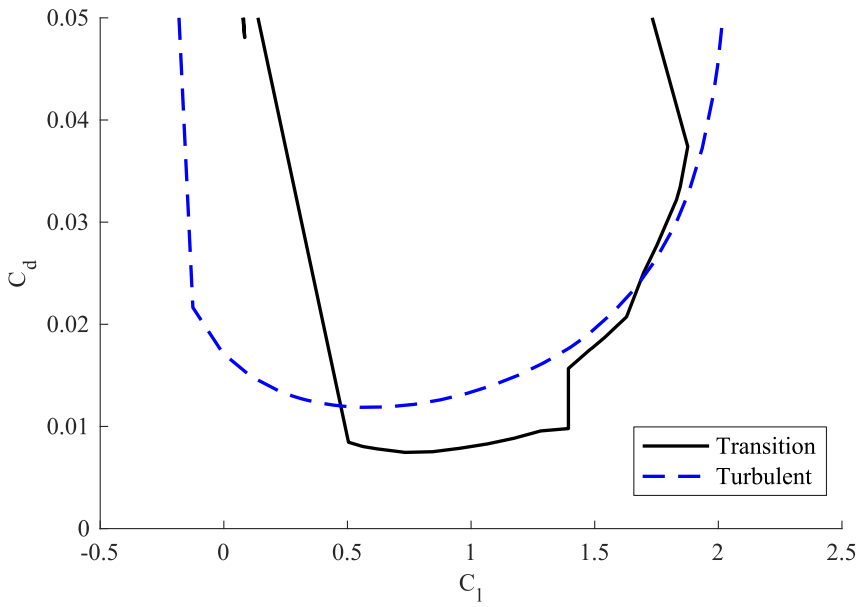

Figure 35 C_d comparison between fully turbulent and transition modeling

When drag coefficients are compared between the models, the transition model shows an area of lower drag. Between lift coefficients of 0.5 and 1.4, the transition model shows approximately 40% less drag. Further analysis of the pressure distributions and skin friction coefficients, show the reason for this drag bucket.

2. Surface Pressure and Skin Friction Distributions

When pressure distributions are compared at 1-degree angle of attack, it is seen that the curves shape are similar, Figure 36. However, the transition model shows a separation bubble near the leading edge of the lower surface, Figure 37,and a bubble near the trailing edge of the upper surface. These bubbles coincide with transition appearing when skin friction coefficient, plotted in Figure 38. On the lower surface, at approximately 20% chord the SST shows flow transitioning. From there to the trailing edge, both models predict nearly identical skin friction coefficients. On the upper surface, transition is delayed to 70% chord and causes the transition model to predict lower skin friction over most of the sail. This deficit causes the reduction in drag coefficient in the SST model.

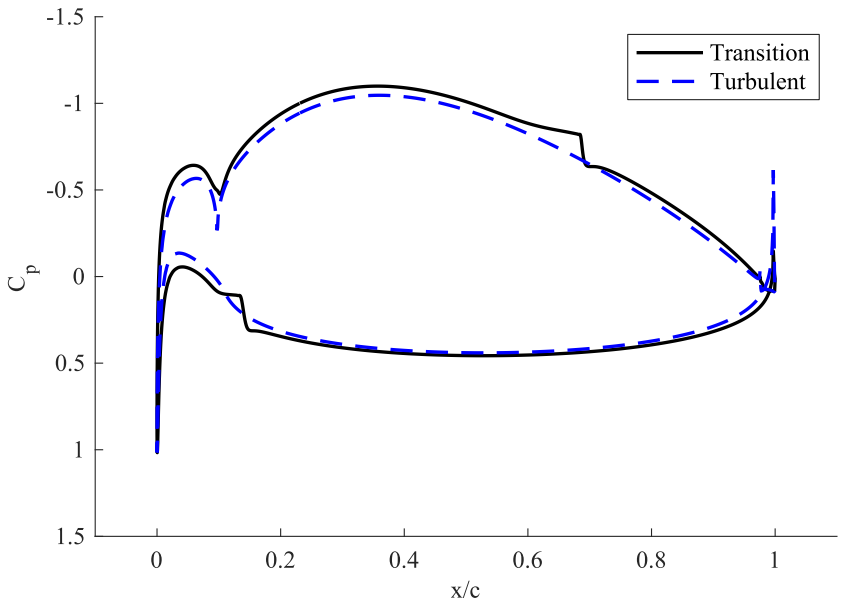

Figure 36 Pressure coefficients at 1-degree angle-of-attack at Re=2,000,000

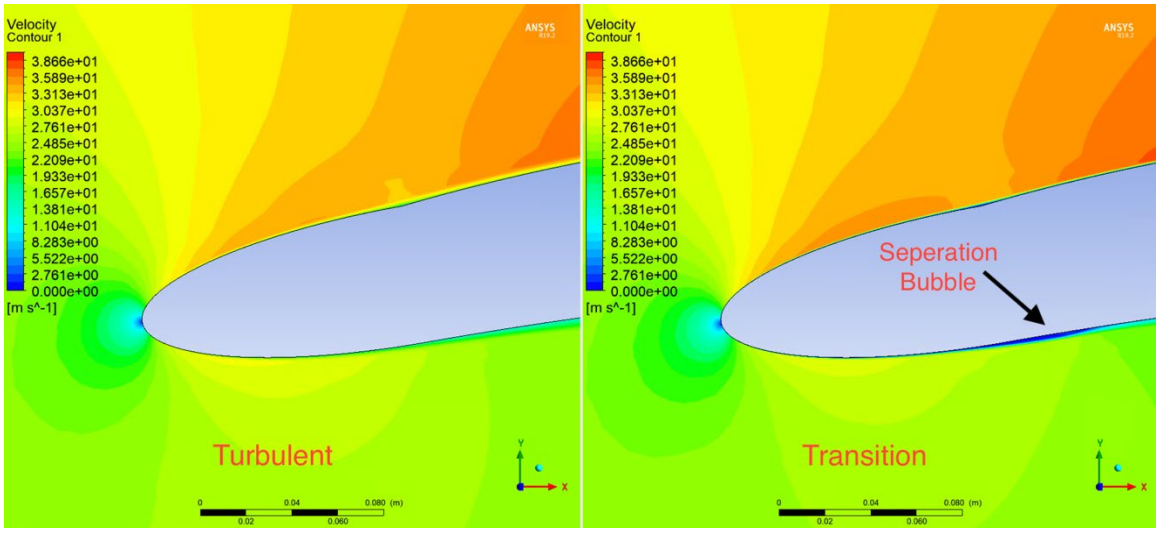

Figure 37 Comparison of leading edge velocity fields at 1-degree angle-of-attack

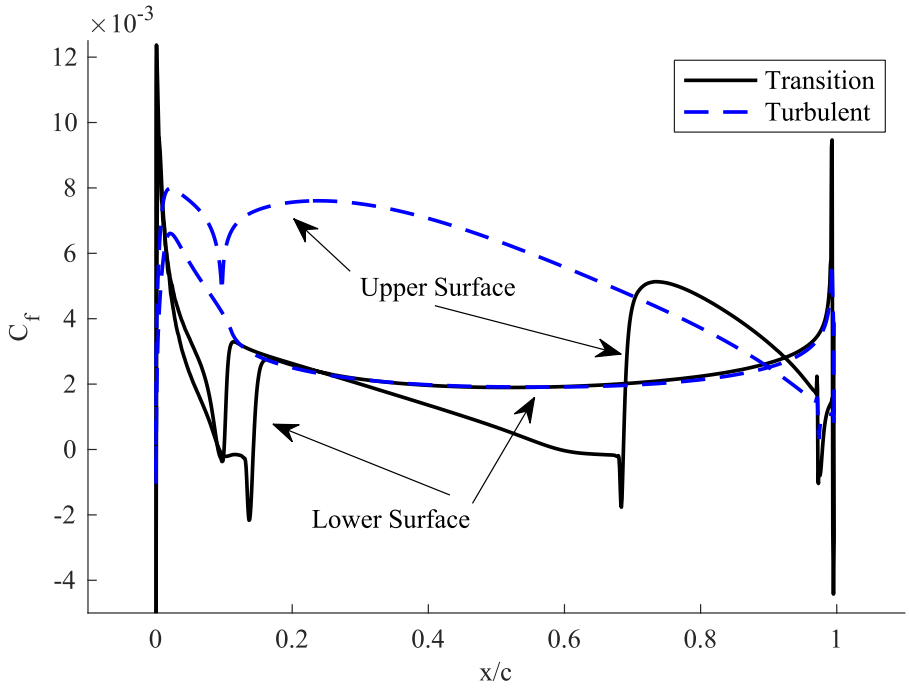

Figure 38 Skin friction coefficient at 1-degree angle-of-attack at Re=2,000,000

This predicted delay in transition on the upper surface disappears as the angle of attack is increased past 5 degrees. By 10-degrees angle-of-attack, SST predicts transition on both the upper and lower surface occurring near the leading edge, Figure 39. This is shown in the pressure distribution, Figure 40, and the skin friction coefficient, Figure 41.

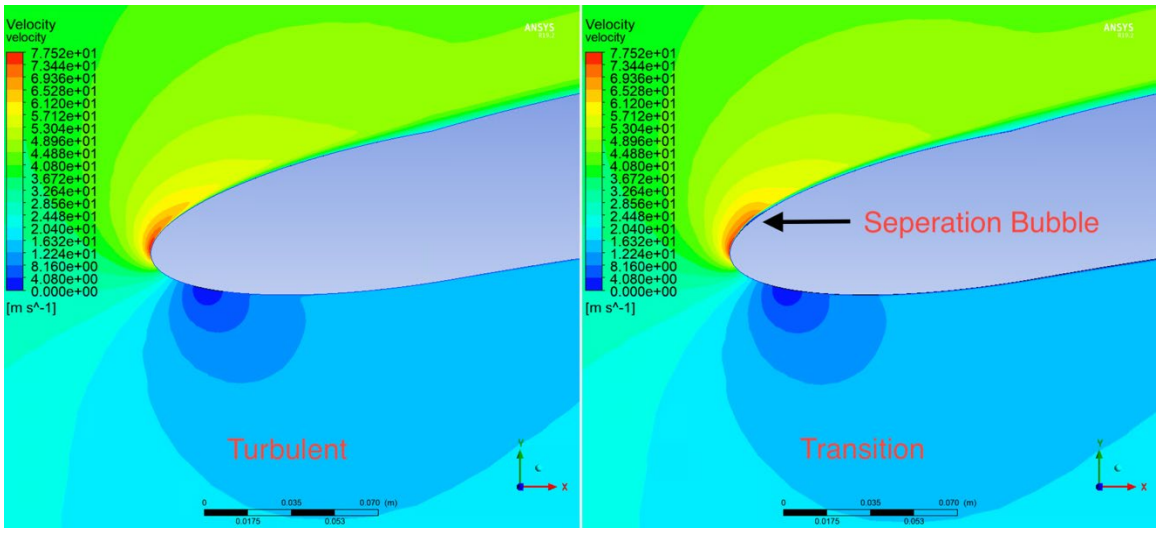

Figure 39 Comparison of leading edge velocity fields at 10-degrees angle-of-attack

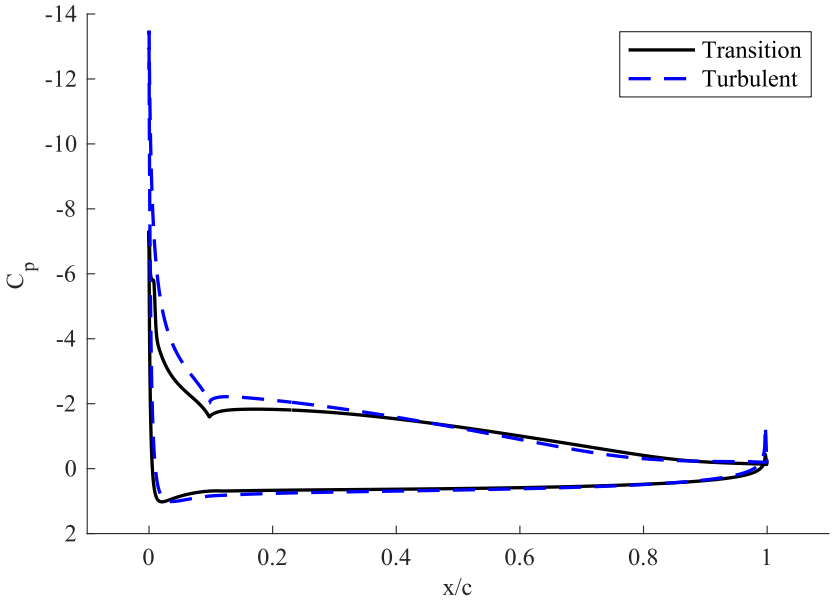

Figure 40 Pressure coefficient at 10-degrees angle-of-attack at Re=2,000,000

The delayed onset of transition predicted by the SST appears to be a result of the discontinuity between the mast and upper surface. In the 1-degree case, the skin friction at this point appears to rise as if the flow is beginning to transition because of this geometric feature. However, at this same point, the flow is accelerating causing a pressure gradient

that acts to promote laminar flow. Not until the flow reaches an adverse pressure gradient near 70% chord does a rise in skin friction signal that SST predicts transition.

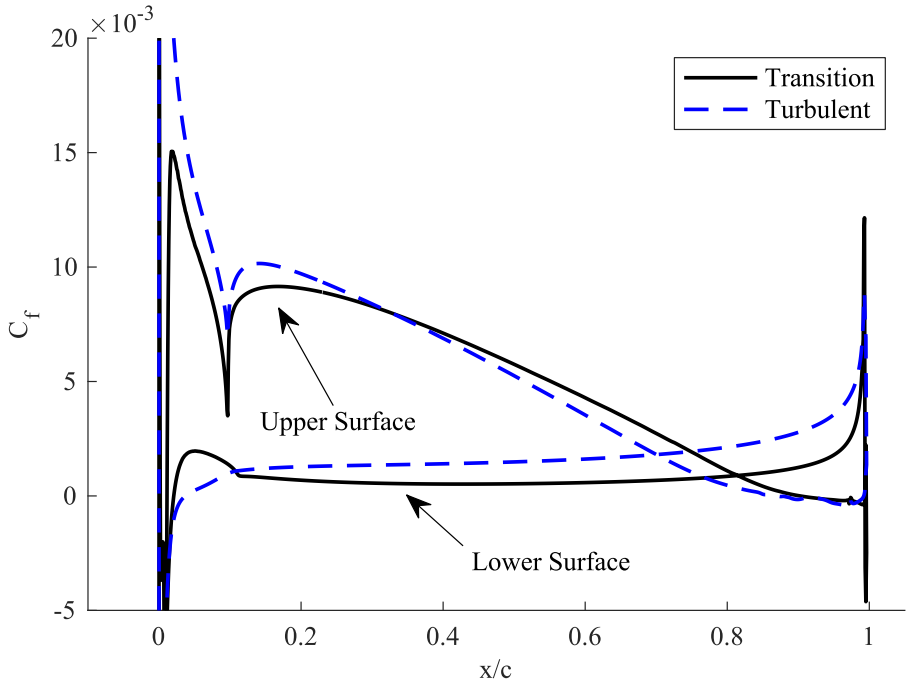

Figure 41 Skin friction coefficient at 10-degrees angle-of-attack at Re=2,000,000

F. TURBULENCE MODEL ASSESSMENT

Though SST predicts great performance, higher lift-to-drag, this performance is unlikely to be seen in actual use of a twin-skin mainsail. Laminar flow on the suction side of the sail is unlikely to be stable in real-world applications. A twin-skin sail will be operating in a constantly varying flow field as the energy pitches and rolls. The angle-of attack and velocity the mainsail will experience will constantly be fluctuating. In addition, surface roughness should promote the development of turbulent flow. Therefore, the κ–ε data are more likely to mirror the real-world performance of the twin skin mainsail.

G. FIGURE OF MERIT

For any given hull shape, a ship will have a peak righting moment that it can supply. Righting moment is the restoring moment that keeps a ship upright and is a function of heel angle for a conventional design. In monohulls, righting moment is achieved from form stability, hull design and ballast placed in the keel. Catamarans generate righting moment from the nature of their hull configuration. As a catamaran heels over and the windward hull is lifted the center of gravity is placed far to windward from the center of buoyancy, thus creating righting moment. Figure 42 shows a typical righting moment curve for both keelboats and catamarans, 1 and 2 respectively.

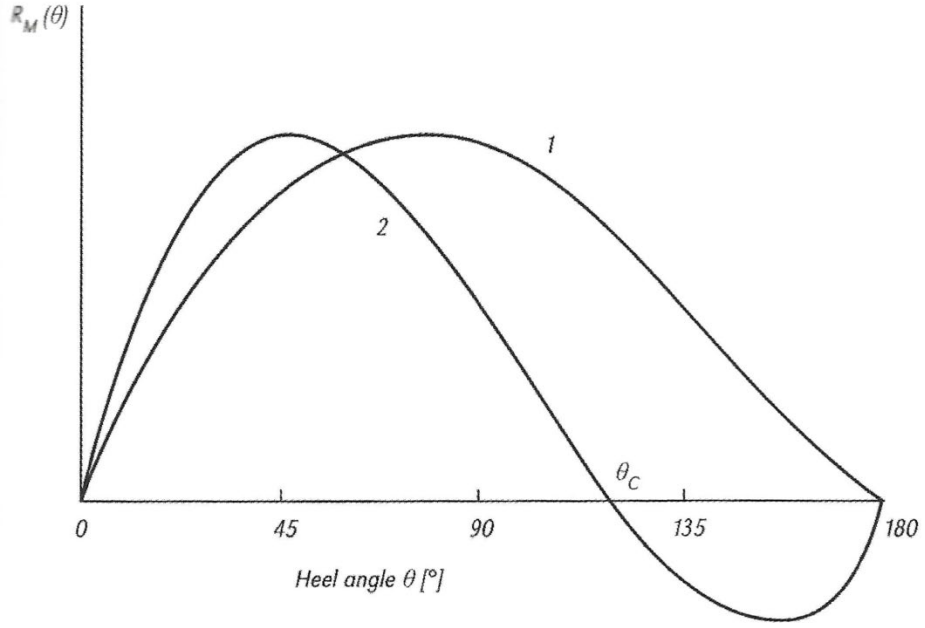

Figure 42 Example righting moment curve. Source: [11].

Every vessel has a maximum righting moment it can deliver by the nature of its design. This aspect of its hull shape and design limits the amount of heeling moment a sailboats' sail plan can generate without capsizing the vessel. Heeling moment is a function of the sailplan's vertical center of effort and the side force generated by the sail. Therefore, to create the most forward speed, a vessel must create the most thrust force for the amount heeling moment its hull design allows it to carry.

To maximize thrust force, the lift to drag ratio of the sailplan and apparent wind angle (AWA), shown in Figure 43, that the vessel sails must be optimized. Figure 44 shows the ratio of thrust coefficient to side coefficient force produced by a nominal sailplan with a given lift to drag ratio over a range of angles of attack. The thrust coefficient is an nondimensional coefficient that describes the force generated by the sail in the direction of motion. The side force coefficient nondimensionally represents the force generated by a sail perpendicular to the direction of motion. For this configuration, maximum thrust for a given constrained value of side force, a physical property of the vessel due to maximum righting moment, occurs at a 90-degree AWA. At this angle, thrust is equal to lift and sideforce is equal to drag. For all other AWAs, the sailboat will create less thrust for a limited side force because both sailplan lift and drag are contributing to the generated side force.

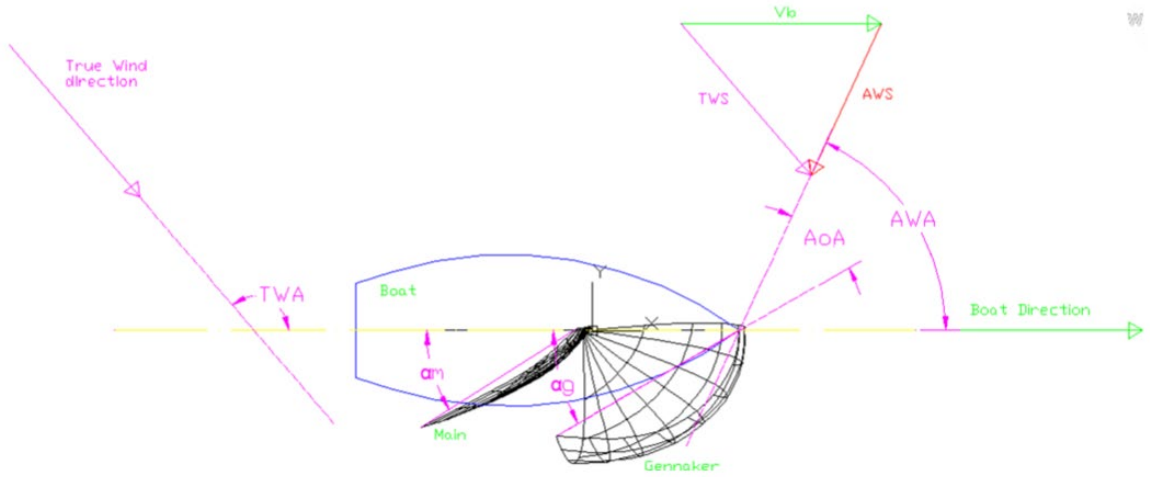

Figure 43 Definition of angles for a sailboat. Source: [10].

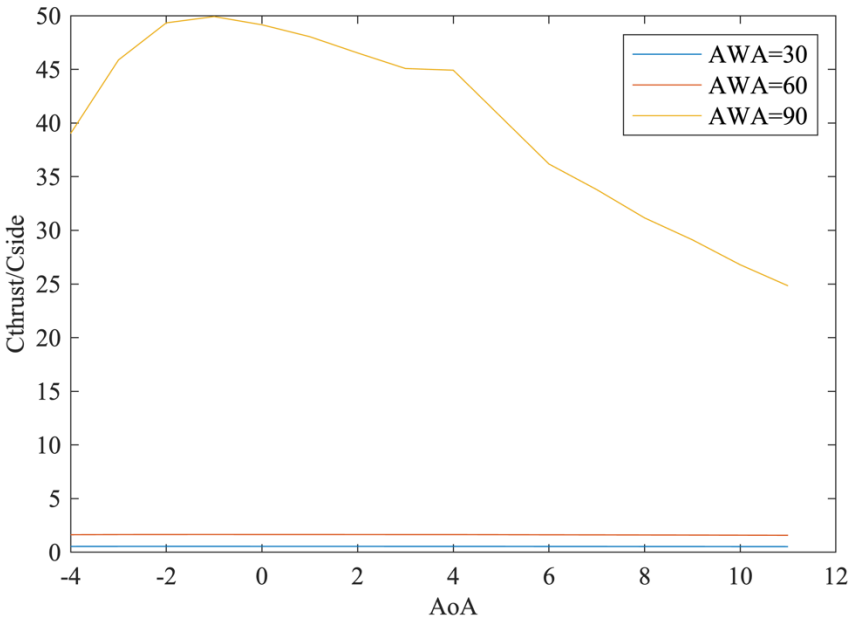

Figure 44 Change in thrust to side force ratio as a function of AWA and AoA

An energy ship desires to create the most thrust in order to create speed through the water to drive the vessel's turbines. Therefore, for energy ship to operate at peak energy collection, the vessel will want to operate at a 90-degree angle of attack or as close to this as possible. In addition. The vessel will want to operate in its maximum lift to drag condition. This dependance on lift-to-drag necessitates the highest lift-to-drag sail designs in order to maximize energy output.

H. COMPARISON TO OTHER DESIGNS

When compared to the lift-to drag results from Johnson's work [4], the twin-skin mainsail, outperforms all designs except the multi-element rigid wing, Figure 45. The higher peak lift-to-drag ratios will allow the twin-skin mainsail to create more thrust both symmetric and single cloth sails.

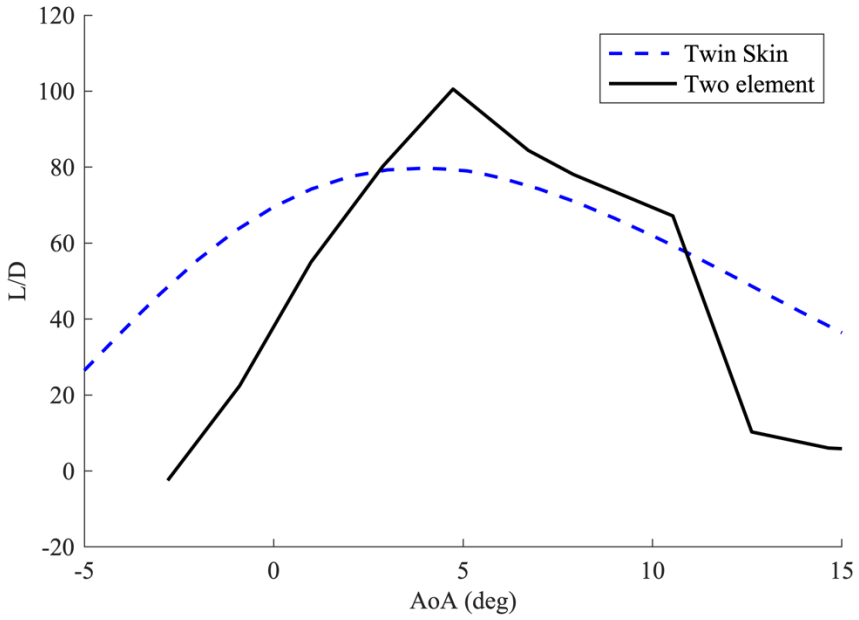

Figure 45 Lift-to-drag results for twin-skin sail compared to two-element wing

I. SUMMARY

The investigation of the twin-skin mainsail showed that it is capable of lift coefficients nearing 2.0. In addition, the drag coefficient estimation was found to vary significantly depending on the choice of turbulence modeling. The discontinuity between mast and sail on the upper surface of the twin-skin mainsail prove an increased challenge for ANSYS CFX in comparison to a typical airfoil. The observed separation bubbles and benign trailing edge stall require future computational and experimental investigations. This investigation is was submitted for publication by IntechOpen [15].

V. CONCLUSIONS AND RECOMMENDATIONS

A. ACCOMPLISHMENTS

A detailed design for the construction of a drag device has been created. All the necessary parts have been ordered. Some progress was made in constructing the test apparatus, particularly in creating the frame to hold the pneumatic cylinder.

Fluid structure interaction was investigated in ANSYS workbench. It was found that FSI can be implemented rather easily using ANSYS software. However, getting stable and physically accurate results proves challenging. It was discovered that computational expense is high for FSI simulations and restricts its use in early stages of design.

In addition, a detailed investigation into the two-dimensional aerodynamics of a twin skin sail has been completed. The simulations included the effect of computational domain size upon the induced circulation around the airfoil. Additionally, both fully turbulent boundary layer flow as well as transitional flow was investigated. It was hypothesized that sailing ships will likely experience fully turbulent flow over most of the sail due to surface roughness and unsteady flow thus rendering these simulations more realistic.

B. CONCLUSIONS FOR TWIN-SKIN MAINSAIL

The ANSYS CFX analysis of two-dimensional flow past twin-skin mainsails presented yielded the following major results:

1. The sail is able to produce lift coefficients up to a maximum of 2.0
2. The drag coefficient predictions vary significantly depending on the choice of turbulence and transition modeling. This was to be expected. Nevertheless, a low drag region is predicted in either case between lift coefficients of zero to 1.4.
3. The twin-skin sail presents the ANSYS CFX analysis with a greater than usual challenge because of the slope discontinuities caused by the

transition from the elliptic leading edge to the upper and lower skins and on the upper surface near the trailing edge.

4. In a previous analysis of the NACA 0012 airfoil [4] the code produced a remarkable agreement with the experiment in the low angle of attack range, thus giving confidence in its ability to predict transitional flows.

5. The prediction of separation bubbles and the onset of stall requires further detailed study. Fully turbulent calculations predict a rather benign trailing edge stall. If validated in future computational and experimental investigations this feature will be very welcome.

The CFD data that is presented has not been validated by comparison to known data sets. Publicly available data sets concerning the performance of twin-skin mainsails do not exist. These data sets may exist within internal team documentation for the 36th America's Cup, but due to the competitive nature of the event, teams have not published their findings. Despite this there is high confidence that the performance estimations presented in this paper are accurate due to validation of the CFX code by Johnson.

It appears likely that the twin-skin mainsail will find further application in highly competitive sailing competitions, such as the America's Cup race. In addition, another application may occur in the operation of autonomous sailing ships equipped with hydrokinetic turbines and electrolyzers to produce hydrogen. As explained in reference 2, such energy ships require highly efficient sails to produce the propulsive power necessary to overcome the turbine drag and maximize energy production.

When deployed on an ocean-going vessel twin-skin sails should offer an advantage over rigid sails because of ease of stowage and operation. Cloth twin-skin sails can be stowed in either the mast or boom section by rolling the cloth within these sections, unlike rigid sails that cannot easily be stowed. This provides a distinct advantage when operating away from shore in extreme weather and sea-states. By optimizing the sail's performance and aerodynamics, it facilitates the overall system optimization including path planning. In the case of a sail assisted cargo vessel, path planning will consist of optimizing the vessels route to take advantage of both weather and sea conditions to minimize fuel consumption.

A detailed investigation into the two-dimensional aerodynamics of a twin skin sail has been completed. The simulations included the effect of computational domain size upon the induced circulation around the airfoil. Additionally, both fully turbulent boundary layer flow as well as transitional flow was investigated. It was hypothesized that sailing ships will likely experience fully turbulent flow over most of the sail due to surface roughness and unsteady flow thus rendering these simulations more realistic.

Based on the success of the most recent America's Cup competition, twin-skin cloth sails appear to be the most suited to high performance as well as ease of use both in raising and lowering the sails. Hence this concept could be used on large ocean-going ships for either primary propulsion or as auxiliary propulsion to reduce overall fuel burn during transit.

C. RECOMMENDATIONS FOR FUTURE WORK

Future work on sail designs for the energy ship could explore a few different avenues. The first is extending the design of the twin-skin mainsail into 3D. Simulation of full scale 3D twin-skin mainsails will provide greater clarity of the true performance of this design when actually constructed. In addition, future studies should explore the affects of multiple twin-skin mainsails mounted close to one another. A future energy-ship would likely not carry a single sail, due to the feasibility of creating enough sail area to propel the craft with a single, very tall sail. An energy ship would more likely have multiple masts and sails, like the concept shown in Figure 46. The circulation effects caused by mounting these sails close to one is another area to explore.

Due to the delays in constructing and deploying the drag device, it has yet to be tested. Future work will involve deploying and testing the device. Data from these tests will be vital in estimating the output of an energy ship.

Figure 46 Rendering of an energy-ship with multiple sails. Source: [16].

APPENDIX A. TECHNICAL DRAWINGS OF DRAG DEVICE

All dimensions in inches.

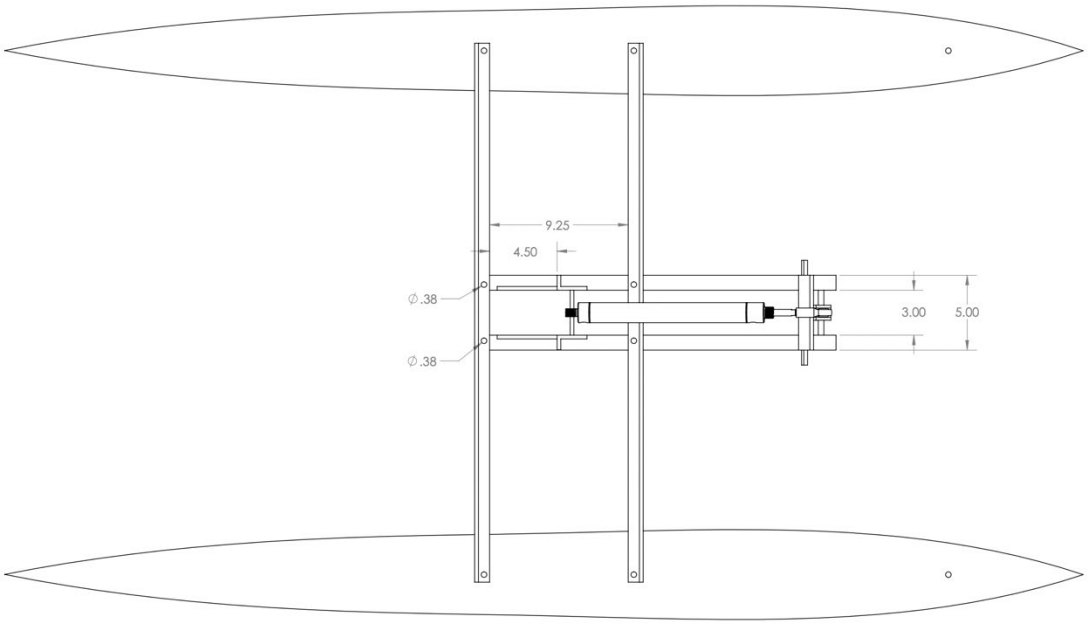

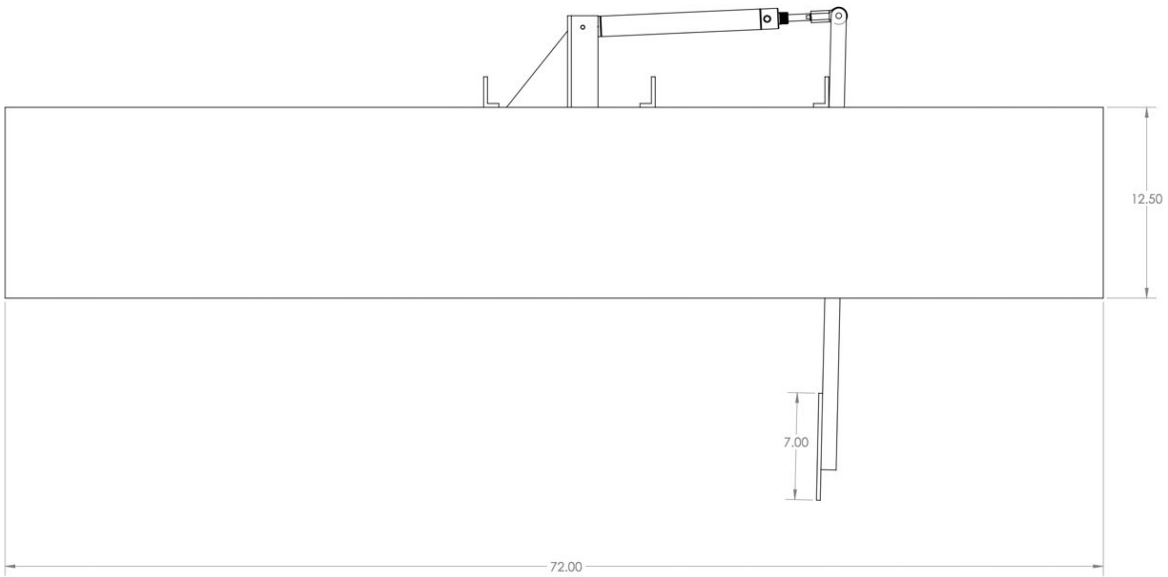

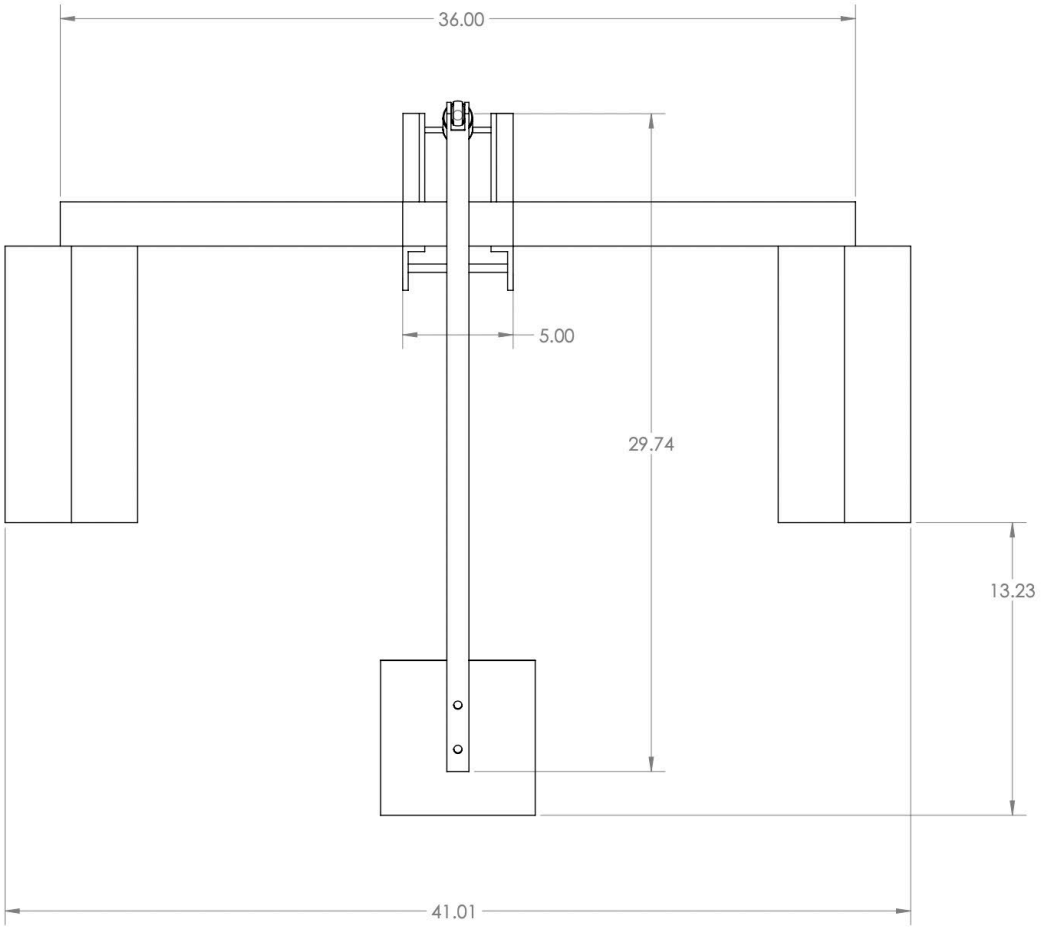
36.00
5.00
29.74
13.23
41.01

APPENDIX B. DRAG PLATE SIZING

A. DESIGN CONDITION

$V = 6\ knots = 3.0867\ m/s$
$Drag = 20\ lbf = 88.964\ N$
$\rho_{seawater} = 1036\ kg/m^3$
$C_{D_{Plate}} = 1.28$

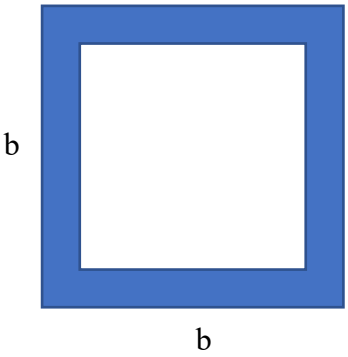

B. CALCULATIONS

$$b = \sqrt{\frac{Drag}{\frac{1}{2}\rho V^2 C_D}}$$

$$b = \sqrt{\frac{88.964}{\frac{1}{2}(1036)(3.0867)^2(1.28)}}$$

$b = 0.11867\ m = 11.87\ cm$

THIS PAGE INTENTIONALLY LEFT BLANK

APPENDIX C. PNEUMATIC SYSTEM CALCULATIONS

```
clear
clc
format compact

Vol_tank= 10* 0.00378541; %10 gal (m^3)
D_cylinder=0.03175; % 1.25in (m)
Stroke=0.2286; %9in (m)
Vol_cyl= pi*(D_cylinder/2)^2*Stroke; % Volume used to move cylinder (m^3)

Hose_length=10; %(m)
D_hose= 0.00635; %0.25in (m)
Vol_hose=Hose_length*pi*(D_hose/2)^2;
R=8.314; %(N/m2)(m3)/K/mol
P(1)= 150*6894.76; %INITIAL TANK PRESSURE 150 psi (Pa)
T=291.483; %65F (K)


%Simulate

n=1;
while P(n)>50*6894.76; %50 psi condition
N(n)=P(n)*Vol_tank/R/T;
P(n+1)= N(n)*R*T/(Vol_tank+Vol_cyl+Vol_hose);
n=n+1;
end

n=[1:length(P)];
plot(n,P)
hold on
plot([0,n(end)],[344738,344738],'r')
xlabel('Cylinder Movements (2*Cycles)')
ylabel('Pressure (Pa)')
legend('Tank Pressure','Limit Condition')
hold off
```

THIS PAGE INTENTIONALLY LEFT BLANK

LIST OF REFERENCES

[1] C. Delbert, "This wind-powered super sailboat will carry 7,000 cars across the atlantic," *Popular Mechanics*, Oct. 07, 2020. https://www.popularmechanics.com/science/energy/a34272175/wind-powered-sailboat-cargo-shipping-future/ (accessed May 20, 2021).

[2] M. F. Platzer and N. Sarigul-Klijn, *The Energy Ship Concept: Renewable Energy from Wind over Water*. Cham: Springer International Publishing, 2021. doi: 10.1007/978-3-030-58244-9_8.

[3] America's Cup, "History of the America's Cup," *36th America's Cup presented by PRADA*. https://www.americascup.com/en/history (accessed May 06, 2021).

[4] R. Johnson , Susan, "Computational aerodynamic analysis of airfoils for energy-producing sailing ships," Naval Postgraduate School, Monterey, 2020. [Online]. Available: https://calhoun.nps.edu/handle/10945/65559

[5] Sailing Anarchy, "The new sailing twin skin setup," *Sailing Anarchy Forums*. https://forums.sailinganarchy.com/index.php?/topic/199608-the-new-sailing-twin-skin-setup/ (accessed May 06, 2021).

[6] G. T. Bryan, "Experimental and computational fluid dynamic analysis of axial-flow hydrodynamic power turbine," M.S. thesis, Naval Postgraduate School, Monterey, 2013.

[7] J. N. Penley, "Gas turbine operation on compressed hydrogen," M.S. thesis, Naval Postgraduate School, Monterey, 2018. [Online]. Available: https://calhoun.nps.edu/handle/10945/61244

[8] Cape Cod Shipbuilding, "Fleet," *Cape Cod Shipbuilding*. https://capecodshipbuilding.com/fleet/ (accessed May 24, 2021).

[9] Sailboat Data, "J/80 sailboat." https://sailboatdata.com/sailboat/j80 (accessed May 24, 2021).

[10] A. Cirello, F. Cucinotta, T. Ingrassia, V. Nigrelli, and F. Sfravara, "Fluid–structure interaction of downwind sails: a new computational method," *J. Mar. Sci. Technol.*, vol. 24, no. 1, pp. 86–97, Mar. 2019, doi: 10.1007/s00773-018-0533-7.

[11] Fabio Fossati, *Aero-Hydrodynamics and the Performance of Sailing Yachts*, 1st Edition. International Marine / McGraw-Hill, 2009.

[12] J. Griffin, "AC75 double luff mainsail," *Sail-World*, Aug. 27, 2018. https://www.sail-world.com/news/209295/AC75-Double-Luff-Mainsail (accessed May 06, 2021).

[13] J. Taglang, “America’s Cup - AC72: The four wings,” *François Chevalier et Jacques Taglang*, Apr. 10, 2013. https://chevaliertaglang.blogspot.com/2013/04/americas-cup-ac72-four-wings.html (accessed May 06, 2021).

[14] L. F. Herreshoff, “Sailboat,” US1613890A, Jan. 11, 1927 Accessed: May 06, 2021. [Online]. Available: https://patents.google.com/patent/US1613890A/en

[15] Sean P. Caraher, Garth V. Hobson, and Max F. Platzer, “Aerodynamic analysis and design of high-performance sails,” in *Modern Ship Engineering, Design and Operations*, Submitted for publication: IntechOpen, 2021.

[16] K. Ouchi and J. Henzie, “Hydrogen generation sailing ship: Conceptual design and feasibility study,” in *OCEANS 2017 - Aberdeen*, Aberdeen, United Kingdom, Jun. 2017, pp. 1–5. doi: 10.1109/OCEANSE.2017.8084808.

INITIAL DISTRIBUTION LIST

1. Defense Technical Information Center
   Ft. Belvoir, Virginia

2. Dudley Knox Library
   Naval Postgraduate School
   Monterey, California